Author Manuscript

Author Manuscript

Author Manuscript

Author Manuscript

HHS Public Access

Author manuscript

Immunity. Author manuscript; available in PMC 2021 November 17.

Published in final edited form as:

Immunity. 2020 November 17; 53(5): 1078–1094.e7. doi:10.1016/j.immuni.2020.09.001.

Affinity-restricted memory B cells dominate recall responses to heterologous flaviviruses.

Rachel Wong[1,2], **Julia A. Belk**[3], **Jennifer Govero**[4], **Jennifer L. Uhrlaub**[2], **Dakota Reinartz**[2], **Haiyan Zhao**[1], **John M. Errico**[1], **Lucas D'Souza**[2], **Tyler J. Ripperger**[2], **Janko Nikolich-Zugich**[2], **Mark J. Shlomchik**[6], **Ansuman T. Satpathy**[3], **Daved H. Fremont**[1], **Michael S. Diamond**[1,4,5], **Deepta Bhattacharya**[2,*]

[1]Department of Pathology & Immunology, Washington University School of Medicine, Saint Louis, Missouri, 63110, USA

[2]Department of Immunobiology, University of Arizona, Tucson, AZ 85724, USA

[3]Department of Pathology, Stanford University School of Medicine, Stanford, CA, 94305, USA

[4]Department of Medicine, Washington University School of Medicine, Saint Louis, Missouri, 63110, USA

[5]Department of Molecular Microbiology, Washington University School of Medicine, Saint Louis, Missouri, 63110, USA

[6]Department of Immunology, University of Pittsburgh School of Medicine, Pittsburgh, PA 15261, USA

SUMMARY

Memory B cells (MBCs) can respond to heterologous antigens either by molding new specificities through secondary germinal centers (GCs) or selecting pre-existing clones without further affinity maturation. To distinguish these mechanisms in flavivirus infections and immunizations, we studied recall responses to envelope protein domain III (DIII). Conditional deletion of activation induced cytidine deaminase (AID) between heterologous challenges of West Nile, Japanese encephalitis, Zika, and Dengue viruses did not affect recall responses. DIII-specific MBCs were contained mostly within the plasma cell-biased $CD80^{+}$ subset and few GCs arose following heterologous boosters, demonstrating that recall responses are confined by pre-existing clonal

*Corresponding author; deeptab@email.arizona.edu.

Author Contributions

D.B., M.S.D., D.H.F., and A.T.S. designed the study. M.J.S. contributed key reagents and technical advice. R.W., J.G., J.L.U., D.R., J.E., L.D.S., and T.J.R. performed experiments. R.W., J.A.B., and D.B. analyzed the data. R.W. and D.B. wrote the paper, and all other authors edited the paper.

Publisher's Disclaimer: This is a PDF file of an unedited manuscript that has been accepted for publication. As a service to our customers we are providing this early version of the manuscript. The manuscript will undergo copyediting, typesetting, and review of the resulting proof before it is published in its final form. Please note that during the production process errors may be discovered which could affect the content, and all legal disclaimers that apply to the journal pertain.

DECLARATION OF INTERESTS

D.H. Fremont is a founder of Courier Therapeutics. M.S.D. is a consultant for Inbios, Vir Biotechnology, NGM Biopharmaceuticals, and on the Scientific Advisory Board of Moderna. The Diamond laboratory has received unrelated funding under sponsored research agreements from Moderna and Emergent BioSolutions. Unrelated intellectual property of D.B. and Washington University has been licensed by Sana Biotechnology. A.T.S is an advisor for Immunai and receives funding support from Arsenal Biosciences. The other authors declare no competing financial interests.

Author Manuscript Author Manuscript Author Manuscript Author Manuscript

diversity. Measurement of monoclonal antibody binding affinity to DIII proteins, timed AID deletion, single cell RNA-sequencing, and lineage tracing experiments point to selection of relatively low affinity MBCs as a mechanism to promote diversity. Engineering immunogens to avoid this MBC diversity may facilitate flavivirus type-specific vaccines with minimized potential for infection enhancement.

Graphical Abstract

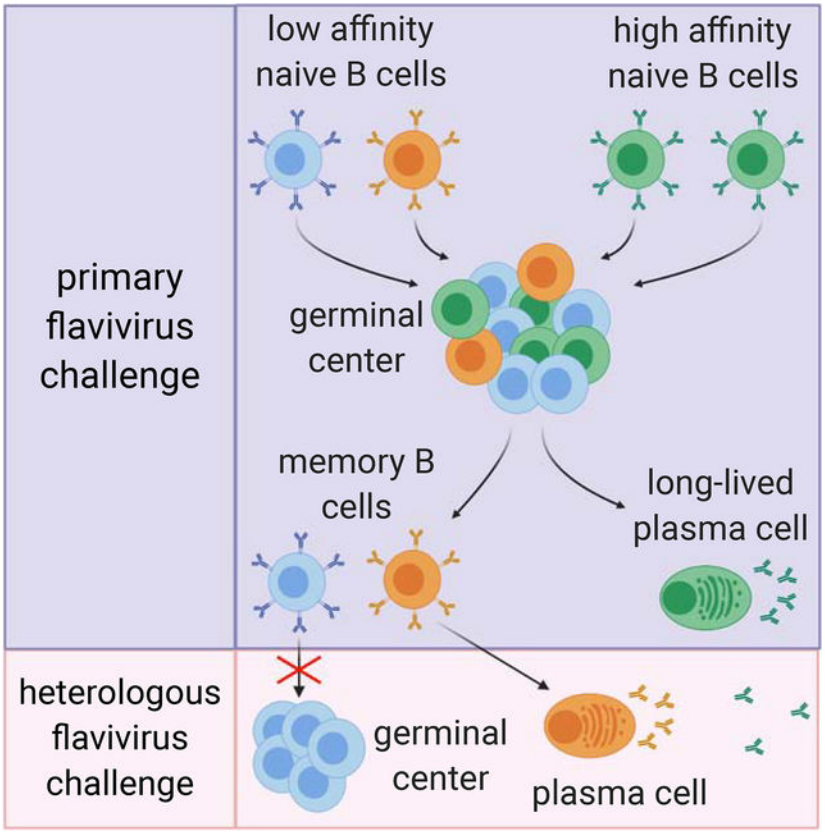

eTOC Blurb:

Memory B cells respond to heterologous antigens either by molding new specificities through secondary germinal centers or by selecting pre-existing clones without further affinity maturation. Wong et al. show that for flavivirus challenges, secondary germinal centers minimally contribute to recall responses. Instead, pre-existing cross-reactive clones are selected from a diverse memory compartment.

INTRODUCTION

After clearance of infections or vaccines, long-lived plasma cells (LLPCs) and memory B cells (MBCs) persist to maintain durable humoral immunity. While MBCs proliferate and differentiate into effector lineages upon antigen re-exposure, LLPCs constitutively secrete antibodies irrespective of the presence of antigen and can provide sterilizing immunity against subsequent homologous or closely related infections (Manz et al., 1998; Slifka et al.,

Author Manuscript Author Manuscript Author Manuscript Author Manuscript

1998). Because of these properties, LLPC-derived circulating antibodies can also sequester antigen that would otherwise activate MBCs (Andrews et al., 2015; Pape et al., 2011). From an evolutionary standpoint, it seems unlikely that MBCs serve solely as an adjunct to LLPCs to bind excess antigen since physiological inocula often are comprised of only a small number of infectious microbes (McNearney et al., 1992). Instead, the most important role of MBCs may be to respond to pathogens that have antigenically changed since the first exposure, thereby evading pre-existing serum antibodies. Hapten-specific MBCs have fewer affinity-enhancing mutations than do LLPCs (Smith et al., 1997; Weisel et al., 2016), providing evidence that the repertoires of these two cell types do not fully overlap. Subsequent work demonstrated that pathogen-specific MBCs have distinct repertoires and distributions of epitope specificities relative to LLPCs (DeKosky et al., 2016; Lavinder et al., 2014; Purtha et al., 2011). These findings led us and others to propose that the diversity of MBCs enables them to combat escape mutants and heterologous viruses better than do LLPCs (Baumgarth, 2013; Purtha et al., 2011; Wong and Bhattacharya, 2019).

In theory, MBCs can respond to heterologous pathogens or escape mutants in two ways. First, the diversity of this compartment may be sufficient to allow the clonal selection of cross-reactive MBCs without additional affinity maturation. Second, MBCs might re-initiate germinal centers (GCs) to shape new B cell receptors (BCRs) tailored to the second heterologous challenge. This decision is mediated by the subset of responding MBCs, which can be functionally distinguished by antibody isotype and, in mice, by additional surface markers such as CD80 and PD-L2 (Bhattacharya et al., 2007; Dogan et al., 2009; Kometani et al., 2013; Krishnamurty et al., 2016; McHeyzer-Williams et al., 2015; Pape et al., 2011; Seifert et al., 2015; Tomayko et al., 2008; Zuccarino-Catania et al., 2014). While adoptive transfer, *ex vivo* culture, and transcriptional profiling experiments have established the differentiation potentials of these MBC subsets in isolation, it is challenging to define how these subsets act in concert and competition with one another *in vivo*.

Mouse and human studies using model antigens or influenza A virus have reached differing conclusions on how efficiently MBCs re-initiate GCs and undergo secondary affinity maturation. In some circumstances, protein-based booster immunizations lead to robust secondary germinal centers and affinity maturation by class-switched memory B cells (McHeyzer-Williams et al., 2015), whereas in other cases this is not observed (Mesin et al., 2020; Pape et al., 2011). Clonal analysis of human influenza A virus infections and vaccinations also have reached different conclusions on whether secondary germinal centers occur and contribute to the recall response (Andrews et al., 2019; Wrammert et al., 2011; Wrammert et al., 2008). These data demonstrate that the specific context of initial infection or vaccination and the nature of the re-challenge defines the type of secondary response.

Flaviviruses represent a particularly relevant system to study recall responses given the co-circulation of many pathogenic flaviviruses such as West Nile (WNV), Japanese encephalitis (JEV), Dengue (DENV), and Zika (ZIKV) and the challenge of antibody dependent enhancement (ADE). ADE is a process by which poorly or non-neutralizing antibodies generated after the first infection enhance uptake of the second heterologous virus in myeloid cells via Fcγ receptors (Acosta and Bartenschlager, 2016; Guzman et al., 2013). Although primary flavivirus infections result in durable homotypic protection (Sabin, 1952),

Author Manuscript Author Manuscript Author Manuscript Author Manuscript

ADE of subsequent infections by heterologous flaviviruses can result in more severe symptoms than if the host were naïve (Halstead et al., 1983; Sangkawibha et al., 1984). It remains unknown whether or how MBCs generated after one flavivirus vaccination or infection respond to poorly conserved neutralizing epitopes of a subsequent heterologous vaccination or infection. The lack of basic understanding of these processes has made designing effective vaccines to DENV and ZIKV very challenging (Halstead, 2017). There are no genetic mouse models that can distinguish the functional importance of secondary GC reactions versus clonal selection of pre-existing diversity without also altering other components of the immune response. Fully addressing these issues in human subjects also is difficult, as it is not feasible to completely sample MBCs prior to heterologous infections.

Here, we used flavivirus infections, vaccinations, and genetic mouse models to examine how MBCs respond to heterologous challenges. We found that abrogating germinal center function minimally impacts recall responses against heterologous flavivirus antigen epitopes, suggesting clonal selection from a diversity of pre-existing MBC specificities with little role for further secondary affinity maturation. This diversity was promoted by the selection of low affinity antigen-specific B cells that were preferentially recruited into the MBC compartment. Restricting the initial diversity through immunogen design may allow for flavivirus type-specific vaccines with minimized potential for infection enhancement.

RESULTS

Plasma cell-biased MBCs recognize and respond to heterologous antigens.

We established a system whereby flavivirus-specific MBCs could be quantified using antigen tetramers. We focused on domain III (DIII) of the flavivirus envelope, as potently neutralizing but weakly conserved lateral ridge epitopes exist within this region (Beasley and Barrett, 2002; Fernandez et al., 2018; Nybakken et al., 2005; Oliphant et al., 2005; Oliphant et al., 2007; Zhao et al., 2016). Bacterially-expressed, site-specifically biotinylated, recombinant DIII was assembled into tetramers with streptavidin-fluorophore conjugates. By analogy to peptide:MHC tetramers, these reagents likely can detect B cell receptors at μM and better affinities, but may miss B lymphocytes that bind antigen more weakly (Martinez et al., 2016). To validate the system, we immunized wild-type mice with Innovator WNV vaccine, an inactivated veterinary vaccine that generates similar antibody responses and specificities as do live infections (Purtha et al., 2011), and analyzed the switched Ig (swIg) $CD80^+CCR6^+$ MBC population. We observed an enriched WNV WT DIII $tetramer^+$ population in the swIg $CD80^+CCR6^+$ MBC population in WNV vaccinated mice compared to naïve mice (Figure S1A).

Depending on the subset of MBCs formed after the resolution of a vaccination or infection, reactivated MBCs can either differentiate into plasma cells or re-initiate GCs. These subsets can be identified using a combination of IgM, IgD, CD80, CCR6, PD-L2, and CD73 markers (Bhattacharya et al., 2007; Dogan et al., 2009; Krishnamurty et al., 2016; Tomayko et al., 2010). PD-L2 and CD73 expression largely overlapped with CCR6 irrespective of immunoglobulin isotype (data not shown), suggesting redundancy between these markers. Thus, we focused subsequent analyses on CCR6 and CD80 expression. We observed that only the swIg $CD80^+CCR6^+$ MBC subset was enriched for WNV DIII-specificity in WNV

Author Manuscript Author Manuscript Author Manuscript Author Manuscript

vaccinated mice relative to unimmunized animals (Figures 1A, S1B). These $CD80^+$ MBCs preferentially generate plasma cells upon re-encounter with cognate antigen (Zuccarino-Catania et al., 2014).

To study how these plasma cell-biased MBCs respond to heterologous challenges, we first tested a WNV-JEV sequential vaccination. WNV and JEV belong to the same serogroup and have a DIII amino acid sequence similarity of approximately 75%. WNV-JEV DIII antibody cross-reactivity was first confirmed by analyzing the swIg $CD80^+$ MBC DIII specificities in WNV-immune mice. After primary vaccination with WNV, we identified a small population of WNV DIII-specific memory B cells that also recognized JEV DIII (Figure 1B). To define shared epitopes between WNV and JEV DIII, we generated point mutations that ablate the LR epitope and abolish binding of potently neutralizing mAbs. For WNV DIII, we incorporated K307E and T330I mutations (KT DIII) (Nybakken et al., 2005; Oliphant et al., 2005), whereas for JEV DIII we introduced 4 LR mutations (E306A/S329I/A366E/K390S, JEV ESAK-DIII) based on previously solved structures (Luca et al., 2012). Proper reactivity and refolding of the JEV ESAK-DIII protein was confirmed by ELISA using the LR-specific neutralizing mAb JEV-31 (Fernandez et al., 2018) and serum from immunized mice (Figure S1C). Thus, B cells or antibodies that bind WT DIII but not mutant DIII were considered DIII-LR-specific, whereas cells or antibodies that bind both WT DIII and mutant DIII likely recognized a distinct non-LR DIII epitope. Further analysis of MBCs following primary WNV vaccination revealed that nearly half of WNV KT DIII-reactive MBCs recognized both JEV DIII-WT and JEV ESAK DIII (Figure 1C). These cells likely cross-reacted with conserved non-LR epitopes between DIII of WNV and JEV. In contrast, only ~1% of WNV DIII-LR-specific MBCs also bound JEV DIII (Figure 1C). These data are consistent with previous mouse and human studies reporting rare but detectable DIII-LR monoclonal antibodies that cross-react with different flavivirus species (Fernandez et al., 2018; Robbiani et al., 2017; Sapparapu et al., 2016; Zhao et al., 2019).

To selectively study secondary MBC responses and not primary responses by naïve B cells, we utilized the Ixiaro JEV vaccine. Ixiaro is an alum-adjuvanted, clinically approved, and formalin-inactivated JEV vaccine, which requires multiple immunizations to elicit a protective antibody response (Dubischar-Kastner et al., 2010). Naïve mice vaccinated with Ixiaro generated few detectable JEV DIII-specific antibodies, whereas WNV-immune mice generated a significant increase in JEV DIII-specific antibodies (Figures 1D and S1D). Most of this response was directed against the non-LR epitope of JEV, as we observed a proportionate increase in WNV KT DIII antibodies after vaccination (Figure 1D). These data demonstrated a robust secondary response to JEV vaccination.

WNV DIII-specific secondary GCs were not detectable after JEV vaccination (Figure 1E), suggesting that recall responses occurred without additional affinity maturation. This was perhaps predictable given the dominance of the swIg $CD80^+CCR6^+$ plasma cell-biased MBC subset (Figures 1A and S1A). To enhance the overall response and formation of other MBC subsets, we infected, rather than vaccinated, mice with WNV-NY99. This infection led to the generation of both GC-competent ($CD80^-$, IgM^+) and plasma cell-biased (swIg, $CD80^+CCR6^+$) WNV DIII-specific MBCs (Figure S1E). Despite the presence of CD80− MBC subsets, these convalescent mice still failed to generate WNV DIII-specific GCs after

Author Manuscript Author Manuscript Author Manuscript Author Manuscript

JEV vaccination (Figure S1F). These data suggested that flavivirus-specific MBCs minimally participated in secondary GCs during recall responses to heterologous challenges.

MBCs do not require additional affinity maturation to respond to heterologous challenges.

Small quantities of DIII-LR antibodies can protect against infection (Purtha et al., 2011). We therefore considered the possibility that MBCs do participate in secondary GCs below our limit of flow cytometric detection and functionally contribute to protective antibody responses. To test this possibility genetically, we developed a mouse model that allows for temporal abrogation of somatic hypermutation, and thus further affinity maturation, between primary and secondary challenges. Mice were generated with loxP sites flanking exon 2 of the *Aicda* gene (Figures S2A–B). *Aicda* encodes activation induced cytidine deaminase (AID), a protein that is critical for class switching and somatic hypermutation (Muramatsu et al., 2000). These mice allowed us to distinguish the contributions of secondary affinity maturation of MBCs versus clonal selection of MBCs with pre-existing specificities, as the former requires expression of AID whereas the latter does not.

Aicda$^{f/f}$ mice were crossed to a tamoxifen-inducible, hCD20-B cell specific Cre recombinase (TamCre) (Khalil et al., 2012) (Figure S2A). To confirm deletion of AID at the protein level, *Aicda*$^{f/f}$ × TamCre (AID cKO) mice were immunized with sheep red blood cells, treated with tamoxifen, and then GC B cells sorted at different time points after tamoxifen treatment. AID protein expression was abolished rapidly after tamoxifen treatment and remained undetectable by immunoblot for at least seven days (Figure S2C). To confirm loss of class switching after AID deletion, AID cKO and *Aicda*$^{f/f}$ (AID WT) mice were treated with tamoxifen for two weeks, vaccinated against WNV, and IgG responses were assessed 12 days later (Figure S2D). As expected, AID cKO mice failed to mount an isotype-switched IgG response to WNV DIII (Figure S2D).

The importance of secondary affinity maturation of MBCs was determined by deleting *Aicda* between WNV and JEV vaccinations. AID WT and AID cKO mice were vaccinated with WNV and the primary response was allowed to proceed. Mice were treated with tamoxifen 56 days later to delete AID, and then re-vaccinated with JEV (Figure 2A). Serum antibody binding to WNV WT DIII, WNV KT DIII, JEV WT DIII and JEV ESAK DIII proteins 14 and 70 days after JEV vaccination was compared by ELISA. Deletion of AID prior to JEV booster vaccination had no discernible effect on serum IgG or IgM titers against LR and non-LR epitopes between days 14–70 of the recall response (Figures 2B–C). As expected from Figure 1C, recall responses were primarily directed against non-LR epitopes, as most antigen-specific antibodies were accounted for by WNV KT DIII and JEV ESAK DIII binding (Figure 2B). However, in both AID WT and AID cKO mice, the levels of JEV WT DIII-reactive antibodies were higher than those against JEV ESAK DIII (Figure 2D). These data suggested that a subset of the MBC response was directed against the neutralizing JEV DIII-LR epitope and occurred independently of AID. Consistent with this interpretation, serum neutralization of JEV was similar between *Aicda* genotypes (Figure 2E). These data demonstrated that rare pre-existing MBCs mediated cross-neutralizing responses without a requirement for further somatic hypermutation and affinity maturation upon heterologous flavivirus challenges.

Author Manuscript Author Manuscript Author Manuscript Author Manuscript

We considered the possibility that additional affinity maturation is necessary for more disparate heterologous challenges. ZIKV, another member of the flavivirus genus, shares ~ 55% DIII amino acid sequence similarity with JEV. We tetramerized recombinant ZIKV DIII to improve avidity, immunized mice, and then followed with JEV vaccination (Figure S3A). Deletion of AID prior to JEV booster vaccination in ZIKV DIII-immune mice did not impact IgG (Figure S3B) or IgM (data not shown) antibodies against ZIKV DIII, JEV DIII, or JEV ESAK DIII. To determine if secondary affinity maturation occurred following heterologous infections, rather than vaccinations, we utilized a sequential DENV and ZIKV infection model (Figure S3C). DENV2 and ZIKV DIII share approximately 46% amino acid similarity. Analysis of ZIKV DIII-specific MBCs and LLPCs, after correcting for naïve B cell responses against ZIKV, again suggested a minimal role for secondary GC reactions and affinity maturation (Figure S3D). These data demonstrate that for responses against both similar and disparate flavivirus DIII-LR antigens, for both vaccines and infections, secondary affinity maturation was minimally involved. Instead, heterologous challenges promoted clonal selection from pre-existing cross-reactive and diverse MBCs.

MBCs are actively selected from GC B cells.

We next sought to define mechanisms by which this MBC diversity was generated during the primary response. Given the results above, we focused on mechanisms by which the $CD80^+$ MBC subset was selected from GCs. As this was the only detectable MBC population following WNV vaccination (Figure 1A), unless otherwise noted, we hereafter refer to this CD80+ subset simply as MBCs. Diversification can be achieved potentially through random selection of GC B cells into the MBC compartment (Tarlinton, 2006). This would result in similar distributions of antigen-specificities in both GC and MBC compartments. However, if active selection were to occur, the antigen-specificity distributions between MBCs and GC B cells might differ. To distinguish these possibilities, wild-type mice were vaccinated against WNV and the DIII specificities in the GC and MBC compartments were quantified by flow cytometry at different time points. GC B cells ($CD19^+GL7^+CD38^-IgD^-$) showed a skewed frequency of WNV DIII-reactive cells towards the LR epitope, although a small fraction of non-LR specific cells was present at stable frequencies throughout the experiment (Figure 3A). In contrast, MBCs were far less skewed towards the WNV DIII-LR epitope (Figure 3B), consistent with previous findings (Purtha et al., 2011). As a result, MBCs had a larger ratio of WNV DIII non-LR:DIII-LR specificities than did GC B cells at all time points analyzed (Figure 3C). Repertoire overlap was observed between germline IgH sequences of DIII non-LR specific GC B cells and MBCs 14 days after WNV vaccination, indicating that these MBCs originate from GC reactions (Figure 3D). To confirm that WNV DIII non-LR specific GC B cells were more predisposed towards the MBC fate, we analyzed the frequency of $CD38^+CCR6^+$ MBC precursor cells within the WNV DIII-LR and WNV DIII non-LR specific GC B cells ($CD19^+GL7^+IgD^-$). CCR6 and CD38 expression mark both mature MBCs and GC precursors committed to the MBC fate (Bhattacharya et al., 2007; Ridderstad and Tarlinton, 1998; Suan et al., 2017). DIII non-LR specific GC B cells had a higher frequency of $CCR6^+CD38^+$ MBC precursor cells compared to WNV DIII-LR specific GC B cells at all time points analyzed (Figure 3E). Thus, although the frequency of WNV DIII non-LR-specific GC B cells was low, these cells were either preferentially selected or maintained within the MBC compartment.

Author Manuscript Author Manuscript Author Manuscript Author Manuscript

MBCs have lower avidity for their antigens than do LLPCs

The mechanism of MBC and LLPC selection from GCs has not been fully resolved. Based on the number of somatic mutations and timing of formation, LLPCs are thought to be selected from high affinity GC B cells (Ise et al., 2018; Kräutler et al., 2017; Phan et al., 2006; Weisel et al., 2016). Several studies have suggested that MBCs also are selected from high affinity GC cells (Polo et al., 2008; Wang et al., 2017), whereas other studies have concluded the opposite (Shinnakasu et al., 2016; Smith et al., 1997; Suan et al., 2017). Adding further complexity, the CD80+ MBC subset, which predominated in our system (Figure 1A, S1B), is formed from GCs at late time points that overlap with those of LLPCs, whereas CD80− MBCs are formed earlier (Weisel et al., 2016). To determine if MBCs in our system have lower affinity or avidity for their antigen compared to LLPCs, we first established methods to identify DIII-specific LLPCs and MBCs. Although plasma cells secrete most of their antibodies, we observed similar expression of surface Igκ as by other B cells in the bone marrow (Figure S4A), consistent with previous studies (Pelletier et al., 2010). We used recombinant DIII tetramers to stain and sort single antigen-specific LLPCs and MBCs (Figures S4A–B), cloned their V(D)J sequences into expression vectors, and then expressed and purified recombinant monoclonal antibodies (mAbs) (Tiller et al., 2009). The cloned mAbs from MBCs and LLPCs were specific for WNV DIII as determined by ELISA and biolayer interferometry. Analogous to the flow cytometry data, 90% of LLPC-derived mAbs were DIII-LR specific compared to 50% for MBC-derived mAbs (Table S1).

We first tested mAbs for their ability to bind monomeric WNV WT DIII. MBC-derived mAbs bound to monomeric WNV WT DIII similarly as mAbs from LLPCs, with modest reductions in binding seen only at the highest concentration of antibody tested (Figure 4A). Reversing the orientation of a subset of the antibodies and WNV WT DIII on the ELISA plate to test affinity rather than avidity also failed to reveal differences between MBC- and LLPC-derived mAbs (Figure S4C). To obtain data on binding kinetics of these mAbs, we performed biolayer interferometry. Affinities and on-rates again were similar between mAbs derived from MBCs and LLPCs (Figures 4B, S4D). If anything, a small reduction in off-rates was observed in MBC-derived mAbs compared to LLPC-derived mAbs (Figure S4D). These data demonstrated that the B cell receptors (BCRs) of MBCs and of LLPCs bound monomeric DIII similarly.

Given that WNV E proteins assemble into rafts of dimers on an icosahedral virion (Mukhopadhyay et al., 2003), we considered the possibility that LLPC-derived mAbs might bind native viral structures better than MBC-derived mAbs. To evaluate this, we tested the avidity of the mAbs to WNV subviral particles (SVPs), which have icosahedral structures similar to fully infectious virions (Ferlenghi et al., 2001; Shen et al., 2018). LLPC-derived mAbs bound with higher avidity to SVPs than MBC-derived mAbs (Figure 4C). This result suggested that an avidity threshold for multimeric flavivirus antigens may have distinguished MBC from LLPC selection in the GC and dictated the breadth of antigens recognized. A lowered avidity threshold, and therefore increased permissiveness to bind variant antigens, in turn could have promoted diversity in the MBC compartment.

Author Manuscript Author Manuscript Author Manuscript Author Manuscript

Absolute affinity thresholds do not segregate MBCs from LLPCs *in vivo*

Our data were consistent with the existence of either an absolute affinity threshold that promoted LLPCs and excluded MBCs, or a relative threshold in which the comparatively lowest affinity B cells within a given GC were allocated to the MBC compartment, perhaps due to the differences in the timing of their selection (Weisel et al., 2016). To determine if an absolute affinity threshold promoted the LLPC fate and resulted in a diverse MBC compartment *in vivo*, we utilized our *Aicda*$^{f/f}$ × TamCre mouse model to freeze affinity maturation at different time points during the GC reaction. We first defined time points at which AID deletion abrogates affinity maturation but not class-switch recombination, and during which MBCs were formed but bone marrow plasma cells had not yet emerged. This is important given differences in IgM and IgG signaling that can influence plasma cell selection (Engels et al., 2009; Ferlenghi et al., 2001; Gitlin et al., 2016; Horikawa et al., 2007; Shen et al., 2018; Waisman et al., 2007; Wan et al., 2015). At both 7 and 14 days after WNV vaccination in wild-type mice, the frequency of WNV DIII-specific GC B cells that had class switched was high (~90%, Figure S5A). This is consistent with recent studies showing that class-switch recombination occurs prior to GC formation (Roco et al., 2019). In addition, the number of somatic mutations in WNV DIII-specific GC B cells increased each week post-vaccination (Figure S5B), demonstrating ongoing affinity maturation.

To determine the kinetics of accumulation of WNV DIII-specific bone marrow plasma cells, ELISPOT assays were performed at different time points after vaccination. We found that WNV DIII-specific bone marrow plasma cells were detectable at 2 weeks post-vaccination and peaked 1 week later (Figure S5C), whereas MBCs emerged earlier (Figure 3B). We deleted AID at 1 or 2 weeks post-WNV vaccination to abrogate affinity maturation temporally and assessed the impact on MBC and LLPC numbers 8 weeks later (Figure 5A). The frequencies of WNV DIII-LR and DIII non-LR specific MBCs were unaffected by AID deletion at weeks 1 or 2 post-vaccination (Figure 5B). Cre expression alone also did not alter antibody responses to WNV WT DIII or WNV E protein (Figure S5D). AID deletion at 1 week after vaccination led to reduced anti-WNV DIII IgG serum antibody titers and slightly reduced numbers of DIII-reactive LLPCs relative to control mice (Figures 5C and S5E). This may indicate an affinity threshold for plasma cell selection, but these data also could be explained by a reduction in the affinity of antibodies and resulting inability to detect all antigen-specific LLPCs. Consistent with the latter mechanism, deletion of AID 2 weeks after WNV vaccination did not affect serum antibody titers or the number of WNV DIII-specific LLPCs (Figure 5C and S5E). Moreover, serum antibodies bound equivalently to multivalent WNV SVPs irrespective of AID deletion (Figure 5D). IgM antibody responses against WNV were also unaffected by AID deletion (Figure S5F). Collectively, these data indicated that an *in vivo* absolute affinity threshold did not exist below which GC B cells were destined to become MBCs. These data are consistent with a recent study showing that AID-dependent affinity maturation is dispensable for LLPC and MBC formation (Gitlin et al., 2016). Notwithstanding this point, our data did not exclude the existence of a relative affinity threshold that segregated MBC and LLPC specificities.

Author Manuscript Author Manuscript Author Manuscript Author Manuscript

Germline affinities of MBC antibodies are lower than those of LLPCs

Previous studies using model antigens and BCR transgenic mice have demonstrated that MBCs and LLPCs of the same specificity have different affinities (Ise et al., 2018; Kräutler et al., 2017; Shinnakasu et al., 2016; Suan et al., 2017; Weisel et al., 2016). Yet how differences in affinity explain changes in specificities between MBCs and LLPCs in a polyclonal response is not immediately obvious. One possible explanation is that the starting populations of B cells destined to become MBCs are distinct from and possess lower avidities than those of LLPC precursors. IgH repertoire analysis during weeks 1–2 of the response revealed similar levels of somatic mutations in the MBC compartment relative to LLPCs (Figure S6A). For reasons that are unclear, the average number of mutations in the MBC population decreased somewhat after week 2 (Figure S6A). We next defined IgH repertoire overlap of MBCs and bone marrow plasma cells at week 4 in the response. As expected, there was little identity between the affinity-matured IgH repertoires of MBCs and LLPCs (Figure 6A). Nonetheless, many plasma cell clones shared a common germline IgH precursor with a small number of clones in the MBC compartment (Figure 6A). In contrast, most germline precursors of MBCs did not reciprocally contribute to the plasma cell compartment (Figure 6A). These results were thus consistent with a more diverse MBC than LLPC compartment.

To directly test germline avidities of LLPCs and MBCs, we reverted somatic mutations in V(D)J regions from our mAbs back to their germline sequences and assessed their abilities to bind monomeric WNV WT DIII and SVPs by ELISA. Germline-reverted MBC-derived mAbs bound more weakly (>10-fold) to WNV DIII and SVPs than did germline-reverted LLPC-derived mAbs (Figure 6B). These data suggest that most MBCs originated from relatively low avidity naïve B cells that were distinct from those of their LLPC counterparts.

Although MBCs might be selected from low avidity GC B cells (Shinnakasu et al., 2016), this does not preclude affinity maturation of their precursors (Wang et al., 2017). Indeed, mutation analysis of our panel of mAbs indicate that MBCs had similar numbers of replacement mutations in their V(D)J genes as did LLPCs (Figure 6C). In fact, MBC clones had slightly greater numbers of silent mutations than did LLPCs, and the total number of mutations were similar between MBCs and LLPCs (Figure S6B). Additional analysis of the MBC mAbs indicated that DIII-LR and DIII non-LR specificities underwent similar selection during GC reactions (Figure S6C). In both the MBC and LLPC compartments, affinity-matured antibodies bound better to monomeric WNV DIII than did their germline-reverted counterparts (Figure 6D). The extent of affinity maturation was difficult to calculate precisely, as many germline-reverted MBC mAbs bound antigen poorly. A similar degree of affinity maturation was observed for binding to WNV SVPs (Figure S6D). Taken together, these data demonstrated that although B cells destined to become MBCs may have begun with low relative affinity, they substantially and rapidly improved their ability to bind antigen during the GC reaction.

We next excluded several affinity-independent explanations for the unique clonal composition of the MBC pool. One possibility is that distinct B cell subsets, such as marginal zone B cells, preferentially contribute to the MBC compartment. However, the antigen-specific precursor frequencies for DIII-LR and DIII non-LR were similar between

Author Manuscript Author Manuscript Author Manuscript Author Manuscript

marginal zone and follicular B cells (Figure S6E). A second possibility is that MBCs emerge from precursors that are more self-reactive than LLPCs. Indeed, in human studies, MBCs tend towards self-reactivity (Scheid et al., 2011; Tiller et al., 2007). However, we observed no changes in the ratios of DIII-LR and DIII non-LR during the transition from Hardy Fractions E-F (Figure S6F), during which self-reactivity is purged (Allman et al., 1993; Goodnow et al., 1988; Hardy et al., 1991; Nemazee and Burki, 1989; Radic et al., 1993; Tiegs et al., 1993). Although WNV DIII-LR cells in Fraction E displayed slightly lower surface levels of IgM, a marker of anergy and self-reactivity (Goodnow et al., 1988), than did WNV DIII non-LR specific cells, these lowered levels were not maintained in the recirculating mature Fraction F cells (Figure S6F). Thus, these avidity-independent mechanisms failed to explain how MBCs acquired specificities distinct from their LLPC counterparts. Instead, we propose that low avidity precursors are preferentially recruited to the MBC compartment.

MBCs are continuously committed from GCs.

Although MBCs and LLPCs had naïve precursor populations with different distributions of avidities and specificities, how these precursors remained biased toward a given fate throughout the GC was unclear. Moreover, the selection of low affinity GC B cells into the MBC compartment was challenging to reconcile with the marked degree of MBC affinity maturation we observed in DIII-specific mAbs, resulting in many MBCs with nanomolar BCR affinities (Figure 4B). We considered two explanations for these observations. First, it was possible that B cells became specified and committed to the MBC fate very early in the response, but still retained GC potential and thus remained in or re-entered GCs to affinity mature. Second, it was possible that MBC commitment occurred continuously from GCs, perhaps from low avidity cells (Shinnakasu et al., 2016). Thus, as GCs improved their overall affinities with time, so too did the pool from which MBCs are selected. To distinguish these possibilities, we first compared different flow cytometric approaches to define committed MBC precursors in germinal centers. $CD38^+$ (Ridderstad and Tarlinton, 1998), $CD38^+EfnB1^+S1PR2^+$ (Laidlaw et al., 2017), and $CD38^+CCR6^+$ (Suan et al., 2017) marker profiles each have been used to identify pre-MBCs alongside standard GC markers. $CD38^+$ GC B cells were enriched for both $CCR6^+$ and $EfnB1^+$ cells whereas $CD38^-$ cells lacked CCR6 expression (Figure S7A). These data demonstrated that pre-MBCs as defined by different groups and markers largely overlapped.

We next performed single cell RNA-sequencing (scRNA-seq) of WNV DIII-specific EfnB1+ GC B cells to transcriptionally identify pre-MBCs and confirm similarity to the MBC precursor population defined by others (Wang et al., 2017). $EfnB1^+$ cells were chosen to exclude activated germinal center precursors, which otherwise express similar markers as pre-MBCs (Laidlaw et al., 2017; Taylor et al., 2012). We recovered high quality scRNA profiles for 2,674 GC B cells which partitioned into six clusters (Figure 7A). We calculated a MBC score for each cell using canonical marker genes (Jash et al., 2016; Shinnakasu et al., 2016; Suan et al., 2017; Wang et al., 2017; Zuccarino-Catania et al., 2014), and visualized this metric on the UMAP plot (Figures 7B–C and S7C). Cluster 4 was enriched for genes associated with MBCs (Laidlaw et al., 2017; Suan et al., 2017; Wang et al., 2017), and also expressed genes consistent with the G1 cell cycle stage and expressed high levels of KLF2

Author Manuscript Author Manuscript Author Manuscript Author Manuscript

(Figure S7B), demonstrating similarity to the pre-MBC population defined previously (Wang et al., 2017). The MBC score was confirmed by visualizing the individual markers, such as CD38, CCR6, and KLF2, (Figures S7B and S7D), further demonstrating similarity to previously defined MBC precursor populations. Finally, we examined clonal relationships between DIII$^+$ pre-MBCs, DIII$^+$ GC B cells, and polyclonal mature swIg CD80$^+$CCR6$^+$ MBCs isolated at Day 7 post-WNV vaccination from the same animals (Figure S7E). We observed extensive clonal overlap of CDR3 regions of both IgH and Igκ between pre-MBCs, mature MBCs, and GC B cells (Figure S7E), consistent with precursor-progeny relationships. Somatic mutation frequencies were similar between pre-MBCs and GC B cells (data not shown).

To functionally test whether committed MBC precursors continued to participate in GCs or were formed continuously *de novo* from GCs, we designed a lineage tracing model. We noted that MBC precursors, but not other GC B cells, lacked expression of Jchain, which can be expressed downstream of or independently of BLIMP1 (Castro et al., 2013) and was expressed in both dark and light zone GC B cells (Figure 7D). We generated mice carrying an IRES-CreERT2 cassette in the 3' UTR of Jchain and crossed them to animals with a ROSA26-loxP-stop-loxP TdTomato cassette (TdT-Jchain mice). Tamoxifen treatment of these mice revealed efficient labeling of GC B cells and bone marrow plasma cells, with negligible labeling of other B cells or non-B lineages (Figure S7F). We reasoned that at early time points post-vaccination, tamoxifen treatment would preferentially mark GC B cells but leave MBC precursors mostly unlabeled. If MBCs at later time points remained similarly unlabeled, these data would imply that low affinity MBC precursors are committed early in the response yet continue to participate in GC reactions (Figure S7G). In contrast, if the percentage of labeled mature and precursor MBCs at later time points were substantially higher than early in the response, this would imply that MBC commitment is not complete early in the response (Figure S7G).

TdT-Jchain mice were vaccinated against WNV, gavaged with tamoxifen at days 5 and 6 after vaccination, and TdTomato expression was analyzed in DIII-specific GCs, MBC precursors, and swIg MBCs at different time points (Figure 7E). Antigen-specific GCs were labeled efficiently, remaining above 60% TdTomato$^+$ at both weeks 1 and 4 post-vaccination. In contrast, few DIII-specific MBC precursors and mature MBCs were labeled at Day 7, with several animals showing no labeling at all in these populations (Figure 7F). By Day 28, the percentages of labeled DIII$^+$ precursor and mature MBCs had increased significantly and were similar to each other (Figure 7F). These data suggested that MBC commitment occurs over time from the GC and was not complete by Day 7 of the response.

In anti-hapten responses, CD80− MBCs arise and complete their formation early in the response, whereas CD80+ MBCs arise later from GCs and with overlapping timing as LLPCs (Weisel et al., 2016). To define the timing of CD80+ MBC formation in our polyclonal system, we treated TdT-Jchain mice with tamoxifen at either 1 or 2 weeks after WNV vaccination. Irrespective of the timing of tamoxifen administration, similar frequencies of labeling were observed within antigen-specific MBC precursors, GC B cells, or mature swIg MBCs (Figure 7G). Together with data above, these results demonstrated

Author Manuscript Author Manuscript Author Manuscript Author Manuscript

that MBC generation began early and continued at least past 2 weeks into the WNV GC response.

DISCUSSION

Unlike LLPCs, MBCs can respond to antigen re-exposure by differentiating into either plasma cells or secondary GC B cells, the latter of which can produce new affinity-matured plasma cells and MBCs. These recall responses may be of particular importance when mutants or genetically divergent strains of pathogens arise that escape serum antibodies. Examples of such pathogens include HIV, which mutates continuously during chronic infections; influenza viruses, which undergo antigenic drifts and shifts; and flaviviruses, in which distinct serotypes co-circulate in overlapping geographic regions. For each of these pathogens, efforts are underway to design vaccine immunogens that would focus the antibody response to neutralizing epitopes. As an example, sequential immunizations are envisioned in which MBCs are gradually guided to the target antibody specificities that bind to antigens such as the CD4-binding site epitopes on HIV (Escolano et al., 2016; Liao et al., 2013; Wu et al., 2011). This strategy assumes the ability of immunogens to engage MBCs to re-initiate GC reactions. Yet in mouse models of heterologous flavivirus challenges, we observed that the MBC compartment was static after WNV vaccination, with little ability to generate new specificities through secondary GCs. This was observed even when the full complement of MBCs was generated by primary infections. Clearly, more details are needed on the cues that allow for the generation and engagement of MBC subsets that can form secondary GCs.

MBCs are diversified relative to LLPCs to ensure greater antigenic coverage than can be achieved by serum antibodies alone. Recent studies on responses to model antigens have provided some potential mechanistic explanations for this property. One model of MBC commitment in GCs correlates with low affinity, lack of T cell help, and Bach2 expression (Shinnakasu et al., 2016). Reciprocally, only the highest avidity cells in the GC receive sufficient T cell help to exit as LLPCs (Ise et al., 2018; Kräutler et al., 2017). Another model of MBC commitment occurs through the interaction of G1-stage GC B cells with IL-9 producing Tfh cells (Wang et al., 2017). In this latter model, MBCs must be of sufficient affinity to receive T cell help. Our results may help reconcile these findings. We observed that the naïve precursors of most CD80+ MBCs begin and end at lower avidity than those of their LLPC counterparts. Yet these cells still undergo affinity maturation and intense selection within the GC. How these models apply to CD80− MBC subsets, which are formed early in GCs prior to LLPCs and CD80+ MBCs (Weisel et al., 2016), remains unclear.

In our system of polyclonal responses to flavivirus vaccinations and infections, there appeared to be two paths for the generation of MBCs from GCs. In the first path, common naïve precursors initiated both MBCs and LLPCs, but there was little to no identity between the repertoires of these cell types as they exited. A second pathway, which accounted for most MBCs in our system, arose from low avidity naïve precursors that did not contribute to the LLPC compartment. That low avidity precursors can contribute to MBCs has been shown in non-competitive transgenic settings (Dal Porto et al., 2002; Dal Porto et al., 1998;

Author Manuscript Author Manuscript Author Manuscript Author Manuscript

Di Niro et al., 2015; Silver et al., 2018), but to our knowledge it has yet to be shown that these initial avidities are predictive of post-GC fate. Irrespective of which path is taken, MBCs eventually emerged with lower average affinities than their LLPC counterparts.

Low relative affinities could increase the breadth of MBC specificities and in several ways. First, the low relative binding capacity of MBCs might allow for affinity maturation in reverse, in which mutations in a pathogen in fact enhance recognition by a subset of MBCs. Our previous work in fact revealed some evidence of such anticipatory memory (Purtha et al., 2011). Second, a low avidity threshold might allow for a greater clonal diversity of MBC specificities, such as those that bind the non-LR epitope, to be recruited into the primary response (Zaretsky et al., 2017). An implication of this mechanism is that immunogen interactions with germline precursors can be manipulated to increase or decrease final MBC and antibody diversity. This agrees with studies that have found other B cell properties, such as proliferation, survival, and GC entry to be linked to germline affinity (Abbott et al., 2018; Anderson et al., 2009; Gitlin et al., 2014; Pape et al., 2018; Paus et al., 2006; Phan et al., 2006; Taylor et al., 2015; Zaretsky et al., 2017).

For flavivirus vaccines, the best strategy might be to restrict antibody and MBC diversity to minimize weakly cross-neutralizing antibodies and ADE, as we found no evidence that such antibodies could be redeemed through secondary GC reactions. Although ‘public’ clonotypes have been isolated from humans infected with closely related flaviviruses (Fernandez et al., 2018; Robbiani et al., 2017; Zhao et al., 2019), our data suggest that such cross-neutralizing antibodies are rare and may already exist prior to heterologous infections. Thus, structure-based immunogen design that minimizes cross-reactive responses, even to otherwise neutralizing epitopes, may achieve flavivirus type-specific immunity while minimizing ADE. Several such efforts are underway already (Frei et al., 2018; Jagger et al., 2019; Richner et al., 2017; Slon-Campos et al., 2019), yet our study offers some additional insight. A ‘hidden’ repertoire of low affinity MBCs exists that is not necessarily reflected in serum antibodies. These MBCs potentially can cross-react with conserved non-neutralizing epitopes across flaviviruses, such as DIII-non-LR and thus yield ADE-promoting antibodies. Given that much of the target population for flavivirus vaccines is seropositive for at least one flavivirus already, special attention might be needed to avoid pre-existing MBCs via immunogen design. Similar strategies have shown initial promise in models of HIV vaccines (Abbott et al., 2018; Havenar-Daughton et al., 2019; Pauthner et al., 2017), and our studies support these approaches for type-specific flavivirus immunizations.

Limitations of study:

First, this is a mouse study. It is possible that the memory B cell subsets induced in humans after infections or vaccinations functionally differ from those in this model system. These questions are challenging to address in humans, but are conceivably possible through before and after repertoire analysis of subjects where different flavivirus strains are endemic. Second, our study focused on the neutralizing DIII-LR epitope, which comprises only a relatively small part of the overall response and is non-trivial to quantify by ELISA or tetramer stains. Finally, our data do not definitively distinguish between high vs. low avidity models of MBC selection from the GC. Rather our data can only support the argument that

Author Manuscript Author Manuscript Author Manuscript Author Manuscript

MBC precursors begin at lower germline avidity than those of their LLPC counterparts. Addressing this question more definitively would require cloning and re-expression of mAbs from pre-MBCs and GC B cells contemporaneously.

STAR METHODS

RESOURCE AVAILABILITY

Lead Contact and Materials Availability—Further information and requests for resources and reagents should be directed to and will be fulfilled by the Lead Contact, Deepta Bhattacharya (deeptab@email.arizona.edu).

Materials Availability—All non-commercially available reagents generated in this study are available upon request.

Data and Code Availability—The accession number for the single cell RNA-seq data reported in this paper in NCBI GEO: GSE154102.

EXPERIMENTAL MODEL AND SUBJECT DETAILS

C57BL/6N, hCD20-TamCre, *Aicda*$^{f/f}$, JchainCreERT2, and B6.Cg-Gt(ROSA)26$^{Sortm14(CAG-tdTomato)Hze/J}$ mice were housed and bred in pathogen-free facilities. All animal procedures used were approved by the Animal Care and Use Committees at Washington University and the University of Arizona. WNV and JEV infections were performed according to A-BSL3 standards. All mice were housed and bred in pathogen-free facilities. Tamoxifen treatment consisted of placing mice on tamoxifen for two weeks. For timed deletions, mice were gavaged for two consecutive days with 50 ug of tamoxifen dissolved in corn oil per gram of mouse weight. Gender and age-matched, 8- to 64-week-old female and male mice were randomly assigned to experimental groups. Littermates were used at controls.

METHOD DETAILS

Generation of Aicda$^{f/f}$xhCD20-TamCre and TdT-Jchain mice.—*Aicda*$^{f/f}$ mice were generated by injecting targeted C57BL/6N embryonic stem line (HEPD0615_4_B08, Aicda$^{tm1a(EUCOMM)Hmgu}$, European Conditional Mouse Mutagenesis Program) into B6 albino (Jackson Laboratory) mice by the Transgenic Knockout Microinjection Core facility at Washington University in St. Louis. Pups were first crossed to ROSA26::FLPe (Jackson Laboratory, Stock No: 003946) mice to remove the LacZ and neomycin resistance sequences, and then to hCD20-TamCre mice (Khalil et al., 2012) to generate *Aicda*$^{f/+}$ mice. Mice were then maintained as either *Aicda*$^{f/f}$ or *Aicda*$^{f/f/}$× hCD20-TamCre and littermates were used as controls. The following primers were used for genotyping the *Aicda* allele: common forward 5'-AGCCCCTCAGCCCTTTAATC-3', wild-type reverse 5'-GCTGGTGTTGTGTGCGAAG-3', *Aicda* targeted 5'-TCGTGGTATCGTTATGCGCC-3'. JchainCreERT2 mice were generated by microinjecting Cas9-gRNA ribonucleoparticles into C57BL6/J zygotes alongside an IRES-CreERT2 donor cassette targeting the 3' UTR of Jchain. The following primers were used for genotyping the *Jchain* allele: Jchain wild-type forward: 5'-TGCTGTGCAGATGATTAGG-3', Jchain transgenic forward: 5'-

Author Manuscript Author Manuscript Author Manuscript Author Manuscript

CCCACATCAGGCACATGAGTAACAA-3', and Jchain common reverse: 5'-CTCCTTGAGCAGACATGAGGATT-3'. Targeted mice were crossed to C57BL6/N mice and then to LoxP-Stop-LoxP (LSL)-TdTomato mice (Jackson Laboratory, Stock No: 007914). Mice heterozygous for Jchain and LSL-TdTomato were used.

DIII refolding and biotinylation—To generated biotinylated DIII, DIII sequences were cloned downstream of a modified pET21 expression vector containing 6x Histidine tag, AviTag (GLNDIFEAQKIEWH), and Thrombin cut site (Nybakken et al., 2005). WNV, ZIKV and JEV DIII proteins were refolded by oxidative refolding as previously described (Fernandez et al., 2018; Oliphant et al., 2007; Zhao et al., 2016). Briefly, BL21(DE3) *E. coli* cells were used for autoinduction of DIII cloned into the pET21 expression vector. The DIII protein was refolded from inclusion bodies by oxidative refolding and purified by size exclusion. AviTagged DIII protein were biotinylated using the NIH Tetramer Core Facility biotinylation protocol (https://tetramer.yerkes.emory.edu/support/protocols#9).

Flow cytometry/sorting—Single cell suspensions were prepared from bone marrow or spleen. Erythrocytes were lysed using an ammonium chloride-potassium solution, and lymphocytes were isolated with Hisopaque-1119 (Sigma-Aldrich) and density gradient centrifugation. Cells were resuspended in PBS with 5% adult bovine serum and 2 mM EDTA prior to staining with antibodies and labeled DIII-tetramers. The following antibodies were purchased from Biolegend: 6D5 (CD19)-Alexa Fluor 700; GL7-FITC -PerCP-Cy5.5, -PE, or Pacific Blue; 90 (CD38)-BV510 or -APC-Cy7; 281–2 (CD138)-PE or -APC; RMM-1 (IgM)-APC; 11–26c.2a (IgD)-PerCP-Cy5.5, -PE-Dazzle594, -BV510, or -BV605; 16–10A1 (CD80)-PE, - Alexa Fluor 488, or -Brilliant Violet 421; 29–2L17 (CCR6)-PE, TY25 (PD-L2)-Brilliant Violet 421 or -PE-Dazzle594; TY/11.8 (CD73)-APC-Cy7; B3B4 (CD23)-BV510; and RA3–6B2 (B220)-FITC. The following antibodies were purchased from eBioscience: 11/41 (IgM)-PerCP-e710 and 4E3 (CD21/35)-FITC. Ephrin-B1-biotin was purchased from R&D Systems. The following antibodies were purchased from Bio X Cell: M1/70 (CD11b), 2C11 (CD3), GK1.5 (CD4), 53–6.7 (CD8), and TER119. Labelled DIII tetramers were generated by incubating biotinylated DIII with labelled streptavidin (Brilliant Violet 421, Brilliant Violet 605, PE, or APC, all from Biolegend) at a 1:4 molar ratio, where $1/10^{th}$ of the total streptavidin was added to DIII every 10 minutes. DIII tetramers were diluted in PBS to 130 ug of DIII/mL, and cells were stained at 2.6 ug/mL of DIII tetramer per 10^7 cells for 20 min on ice. Antigen-specific MBCs and GC B cells were enriched by depleting non-B cells, IgM^+ and IgD^+ splenocytes cells by cellular panning. Splenocytes were stained with rat anti-CD4, CD8, CD11b, CD3, Ter119, IgM, and IgD on ice for 20 min, wash, and then incubated on plates pre-coated with 1 ug/mL of mouse anti-rat IgG (3053–01, Southern Biotech) for 20 min at 4°C. The non-adherent cell fraction was collected, washed, and then stained with MBC and GC B cell surface markers (CD19, GL7, CD38, CD80, CCR6 and DIII tetramers). Antigen-specific bone marrow plasma cells were subjected to CD138 enrichment prior to DIII-tetramer staining. Total bone marrow cells were stained with anti-CD138 APC, cells washed and then stained with anti-PE magnetic beads (0.5 uL/10^7 cells, Miltenyi Biotec). Positive enrichment of CD138-expressing cells was performed using MACS LS columns (Miltenyi Biotec), where enriched cells were stained with 2.6 ug/mL of DIII tetramers.

Author Manuscript Author Manuscript Author Manuscript Author Manuscript

ELISA.—ELISA plates (9018, Corning) were coated overnight at 4°C in 0.1 M sodium bicarbonate buffer, pH 9.5 containing 5 ug/mL of the appropriate domain III antibody, WNV E protein, or 4G2 mAb. All other incubation steps were performed at room temperature for 1 hour. Wash steps were performed between each step using PBS + 0.05% Tween-20. Plates were blocked with PBS + 2% BSA followed by serial dilutions of serum. Plates coated with 4G2 were further incubated with media containing WNV SVPs. Serum was probed with 0.1 ug/mL of biotinylated anti-mouse IgG (715-065-151, Jackson ImmunoResearch Laboratories) or 0.14 ug/mL of biotinylated anti-mouse IgM (115-065-075, Jackson ImmunoResearch Laboratories) and then detected with streptavidin conjugated horseradish peroxidase (554066, BD biosciences). MAbs were probed with 0.8 ug/mL of peroxidase conjugated anti-human IgG (709-035-149, Jackson ImmunoResearch). Plates were developed using TMB (J61325, Alfa Aesar) and neutralized with 2N H_2SO_4. Optical density (OD) values were measured at 450 nm. Serum endpoint titer was defined as the inverse dilution factor that is three standard deviations above background using variable slope measurements and Prism software (GraphPad Software). OD values from mAbs were normalized to the OD values of humanized E16 (NR-31082, BEI Resources) at each dilution.

Neutralization Assays.—Serum was heat-inactivated at 56°C for 30 min. Serial dilutions of serum or mAbs were incubated with 100 FFU of WNV-NY99 (Lanciotti et al., 1999) or JEV SA14-14-2 (Song et al., 2012) for 1 h at room temperature. Serum/mAbs-virus complexes were added to a monolayer of Vero cells in a 96-well plate and incubated at 37°C with 5% CO_2 for 1 h. Cells were overlaid with 1% (w/v) carboxymethycellulose (Sigma-Alrich) in MEM supplemented with 2% FBS, 1x Pen-Strep, and 1x GlutaMax. Plates were harvest 24 (WNV) or 36 (JEV) h later and fixed with 1% PFA in PBS. Plates were incubated with 500 ng/mL of hE16 (for WNV, BEI) or JEV-31 (Fernandez, E. et al., mBio, 2018) diluted in PBS + 0.1% saponin+0.1% BSA. hE16 was detected using 0.8 ug/mL of peroxidase conjugated anti-human IgG, whereas JEV-31 was detected using 100 ng/mL biotinylated anti-mouse IgG followed by streptavidin-HRP. Foci were visualized using TrueBlue peroxidase substrate (50-78-02, KPL) and enumerated on the CTL ImmunoSpot S6 Analyzer.

ELISpot Assays.—ELISpot plates (MSHAN4510, Millipore Sigma) were coated with 10 ug/mL of anti-mouse Ig kappa (559749, BD biosciences) in PBS overnight at 4°C. Plates were blocked with complete DMEM for 1 h. Bone marrow plasma cells were enriched on CD138 as described above and plated in triplicates. Cells were incubated at 37°C with 5% CO_2 for 16 h. Plates were washed with PBS followed by PBS+0.05% Tween-20, incubated with 5 ug/mL of biotinylated WNV WT or KT DIII diluted in PBS, 2% adult bovine serum and 0.05% Tween-20 and incubated at room temperatures for 1 h. Plates were rinsed with PBS + 0.05% Tween-20 and then incubated with streptavidin HRP diluted in PBS, 2% adult bovine serum, and 0.05% Tween-20 at room temperatures for 1 h. Wells were washed one last time with PBS + 0.05% Tween-20 and PBS. Spots were developed using TrueBlue peroxidase substrate and enumerated on the CTL ImmunoSpot S6 Analyzer. The total number of DIII-specific bone marrow plasma cells was calculated by multiplying the

Author Manuscript Author Manuscript Author Manuscript Author Manuscript

number of enumerated spots by the plating dilution factor. The value was then divided by the total number of bone marrow cells.

WNV SVP production.—Lenti-X 293T cells were transfected with WNV prM-E construct (Zhang et al., 2016) using GeneJuice transfection reagent. Supernatants were collected 48 h later, filtered using a 0.2 um filter, aliquoted, flash frozen, and stored at −80°C.

Immunizations.—Mice were administered two doses of inactivated WNV Innovator vaccine (Valley Vet Supply) by intraperitoneal injection on days 1 and 2 (Purtha et al., 2011). Biotinylated ZIKV WT (Zhao et al., 2016) and A310/T335 (LR mutant) DIII were tetramerized with streptavidin at a 1:4 molar ratio, where 50 ug of tetramer was mixed with 100 uL of AddaVax vaccine (Invivogen) and then administered to mice by intraperitoneal injection.

MAb generation and purification.—Antigen-specific MBCs were sorted using a FACSAria II and cultured as previously described (Purtha et al., 2011). Briefly, each well of a 96-well plate were seeded with 30,000 mitomycin C-treated BAFF + CD40L + NIH 3T3 cells (Purtha et al., 2011), one day prior to seeding individual MBCs. Sorted MBCs were co-cultured with the feeder cells in the conditioned 3T3 complete DMEM medium (DMEM, 10% FBS, 1x penicillin-streptomycin, 1 mM sodium pyruvate, 1x nonessential amino acids, and 2 mM GlutaMax) containing 1 μg/ml pokeweed mitogen lectin (Sigma-Aldrich), 10 μg/ml lipopolysaccharide (from *E. coli* 0.111:B4; Sigma-Aldrich), 1 μg/ml phosphorothioated murine CpG (5′-TCCATGACGTTCCTGATGCT-3′; Integrated DNA Technologies), 16 ng/ml mIL-2, 10 ng/ml mIL-6, 17 ng/ml mIL-10 (PeproTech), 10 mM HEPES, and 50 μM β-mercaptoethanol). Supernatant was collected after 6 days of culture, and DIII specificity assessed by ELISA. V(D)J sequences were amplified as described in (Tiller, 2009) and cloned into modified heavy (Addgene plasmid # 8079) and light chain (Addgene plasmid # 80796) expression vectors (Tiller et al., 2008). The modified heavy chain expression contains a G4S linker sequence and an AviTag sequence at the 3’ end of the hIgG1 sequence. Single antigen-specific LLPCs from the bone marrow were sorted into catch buffer containing 0.1M Tris pH 8.0 and RNase inhibitor (Smith et al., 2009) and flash frozen. V(D)J sequences were isolated according to a previously published protocol (Ho et al., 2016). Briefly, cDNA was generated, two rounds of nested PCRs performed to amplify the V(D)J sequences, and then V(D)J sequences cloned into the modified heavy and light chain expression vectors.

Lenti-X 293T cells (Clontech) used for transfections were maintained in complete DMEM containing 10% ultra-low IgG FBS (ThermoFisher), 1x penicillin-streptomycin, 1 mM sodium pyruvate, 1x nonessential amino acids, and 2 mM GlutaMax. Transfections were performed using GeneJuice (EMD Millipore Novagen). Somatically hypermutated mAbs were produced by co-transfecting heavy chain construct, light chain construct, and a BirA ligase construct. Germline reverted mAbs were produced by co-transfecting heavy and light chain constructs. Fresh media was supplemented every other day. Six days after transfection, supernatants were collected, cellular debris filtered, and then mixed with Protein G IgG Binding Buffer (Thermo Scientific) at a 1:1 ratio. MAbs were purified from the supernatant

Author Manuscript Author Manuscript Author Manuscript Author Manuscript

by Protein G (Cytiva) affinity chromatography. Purified antibodies were concentrated and buffer exchanged with PBS containing 0.1% sodium azide using an Amicon® Ultra-15 Centrifugal Filter Unit (30 kDa membrane).

BLI Binding Assays.—The binding affinity of affinity matured mAbs to WNV WT DIII was assessed by BLI using an Octet Red384. The buffer used contained 150 mM NaCl, 10 mM HEPES, 3 mM EDTA, 0.005% Tween20, and 1% BSA, pH 7.4. Biotinylated mAb was loaded onto streptavidin biosensors (ForteBio) at 5 ug/mL for 3 minutes. The association and dissociation of antibody to WNV WT DIII was measured at 30°C. Data were analyzed using the ForteBio DataAnalysis 11.0 software, and fitted to a 1:1 binding model.

IgH repertoire analysis.—WNV DIII-specific GC B cells ($CD19^+GL7^+IgD^-CD38^-$), bone marrow plasma cells ($CD138^+$), and MBCs ($CD19^+GL7^-IgM^-IgD^-CD80^+CCR6^+$) from WT mice were sorted 7, 14, 21, and 28 days after WNV vaccination. RNA was using the NucleoSpin RNA XS kit (Macherey-Nagel) per manufacturer's instructions. cDNA synthesis was performed as previously described (Ho et al., 2016). IgG immunoglobulin transcripts were amplified with the following primers: msVHEstdseq1 5'-ACACTCTTTCCCTACACGACGCTCTTCCGATCTGGGAATTCGAGGTGCAGCTGCAGGAGTCTGG-3' and commonCgstdseq2 5'-GTGACTGGAGTTCAGACGTGTGCTCTTCCGATCTCARKGGATRRRCHGATGGGG-3'. A final amplification with P5 forward Stdseq1 and P7 reverse Stdseq index primers were used as previously published (Lam et al., 2018). Samples were pooled, purified, and then sequence dusing Illumina Miseq v3 2×250 platform using previously published (Lam et al., 2018). Forward and reverse reads were paired using the default settings of PEAR (Zhang et al., 2014). Paired reads were further analyzed using Migmap (https://github.com/mikessh/migmap) where full length VDJ sequences were merged and corrected for PCR errors. Samples were further filtered by excluding non-productive B cell receptors, transcripts without an assigned D gene, and counts below 10. In addition, the maximum number of clones included in subsequent analysis was the number of cells sorted based on the BD FACSAria III. Sequences analyzed using IMGT/HighV-Quest (Lefranc et al., 2009). Duplicate transcripts due to sequencing errors were removed by combining sequences that share the same CDR1, FR2, CDR2, FR3, CDR3, N1-region, P5'D, P3'D, and N2-region nucleotides.

Germline clonal identity was determined by comparing IgH transcripts for the same V gene, D, gene, J gene, N1-region, P5'D, P3'D, and N2-region nucleotides. Clonal identity at the affinity matured state was determined by comparing sequences for the same CDR1, FR2, CDR2, FR3, CDR3, N1-region, P5'D, P3'D, and N2-region nucleotides sequences. Clonal overlap between the different samples were visualized using BioCircos (Cui et al., 2016).

Immunoblotting.—*Aicda*$^{f/f}$ TamCre and *Aicda*$^{f/f}$ mice were immunized with 8×10^8 sheep red blood cells (Lampire) by intraperitoneal injection. GC B cells were sorted on a FACS Aria II at different timepoints after immunization. Cells were lysed in Laemmli buffer containing 2% SDS and 5% 2-mercaptoethanol and stored at −20°C until analysis. Cell lysates were separated by 10% SDS-PAGE and transferred to PVDF membrane (Roche). The membranes were probed with 20 ug/mL of anti-AID monoclonal antibody (mAID-2,

Author Manuscript Author Manuscript Author Manuscript Author Manuscript

eBioscience). The signal was detected using a Luminata HRP substrate (Millipore). Signal from the horseradish peroxidase was quenched by incubating the membrane with 30% H_2O_2 for 10 min. The membrane then was probed with anti-ERK2 (Santa Cruz, C-14) antibody as a loading control. The signal was detected using a Luminata HRP substrate.

scRNA-seq analysis.—WNV DIII-specific GC B cells ($CD19^+GL7^+EphrinB1^+IgD^-$) were sorted using a FACS AriaII and prepared and processed according to 10x Genomics instructions for Single Cell Protocols Cell Preparation Guide and Chromium Single Cell V(D)J Reagents kit. Reads were processed and aligned to the mm10 reference genome using the 10X cellranger count pipeline. The filtered counts matrix was loaded into Seurat (Stuart et al., 2019) for the rest of the analysis. Doublet scoring was performed using `rscrublet`, the R implementation of scrublet (Wolock et al., 2019). High quality cells were determined based on quality control thresholds of <5% mitochondrial reads, a doublet score <0.20, and >200 unique features. A small number of non-B cells were identified and filtered for quality control. Normalization, clustering, dimensionality reduction, and visualization were performed using Seurat and ggplot2. Scores for gene modules were computed using `Seurat::AddModuleScorè. The MBC score is comprised of *Klf2*, *Zbtb32*, *Bach2*, *Il9r*, *Ccr6*, *Cd38*, and *S1pr1*. Cell cycle phase prediction was performed with the `Seurat::CellCycleScoring` function.

Infection.—Wild-type mice were inoculated via subcutaneous injection in the footpad with 10^3 plaque-forming units (PFU) of WNV-NY99 strain, and all experiments were performed in A-BSL3/BSL3 facilities. AID WT and AID cKO mice were inoculated via intraperitoneal injection with 10^6 PFU of ZIKV (Dakar strain 41519, (Zhao et al., 2016), DENV-2 (strain D2S20, (Makhluf et al., 2013), or both.

QUANTIFICATION AND STATISTICAL ANALYSIS

Student’s two-tailed t test, Mann-Whitney test, and 2-way ANOVA were performed using Prism software (Graphpad). Figure legends specify the test used, criteria for statistical significance, and the number of experimental, biological, and technical replicates.

Supplementary Material

Refer to Web version on PubMed Central for supplementary material.

Acknowledgments

This work was supported by NIH grants R01AI099108 (D.B.), K08230188 (A.T.S), P01AI106695 (M.S.D.), R01AI132186 (M.S.D.), R01AI127828 (M.S.D.), and R01AI073755 (D.H.F. and M.S.D.). R.W. was supported by the NSF Graduate Research Fellowship Program (DGE-1143954). J.A.B. was supported by a NSF Graduate Research Fellowship and a Stanford Graduate Fellowship. T.J.R. was supported by NIH predoctoral training grant T32AG058503. A.T.S. was supported by a Bridge Scholar Award from the Parker Institute for Cancer Immunotherapy, a Technology Impact Award from the Cancer Research Institute, and a Career Award for Medical Scientists from the Burroughs Wellcome Fund. We thank the Speed Congenics Facility of the Rheumatic Diseases Core, supported by NIH grant P30AR048335. Flow cytometry experiments reported in this publication were supported by the National Cancer Institute of the National Institutes of Health under award number P30CA023074. We thank Chris Nelson and Melissa Edeling for technical support. We thank the Bioinformatics Shared Resource at the University of Arizona for assistance in bioinformatics analysis.

Author Manuscript Author Manuscript Author Manuscript Author Manuscript

REFERENCES

Abbott RK, Lee JH, Menis S, Skog P, Rossi M, Ota T, Kulp DW, Bhullar D, Kalyuzhniy O, Havenar-Daughton C, et al. (2018). Precursor Frequency and Affinity Determine B Cell Competitive Fitness in Germinal Centers, Tested with Germline-Targeting HIV Vaccine Immunogens. Immunity 48, 133–146 e136. [PubMed: 29287996]

Acosta EG, and Bartenschlager R (2016). Paradoxical role of antibodies in dengue virus infections: considerations for prophylactic vaccine development. Expert Rev Vaccines 15, 467–482. [PubMed: 26577689]

Allman DM, Ferguson SE, Lentz VM, and Cancro MP (1993). Peripheral B cell maturation. II. Heat-stable antigen(hi) splenic B cells are an immature developmental intermediate in the production of long-lived marrow-derived B cells. J Immunol 151, 4431–4444. [PubMed: 8409411]

Anderson SM, Khalil A, Uduman M, Hershberg U, Louzoun Y, Haberman AM, Kleinstein SH, and Shlomchik MJ (2009). Taking advantage: high-affinity B cells in the germinal center have lower death rates, but similar rates of division, compared to low-affinity cells. J Immunol 183, 7314–7325. [PubMed: 19917681]

Andrews SF, Huang Y, Kaur K, Popova LI, Ho IY, Pauli NT, Henry Dunand CJ, Taylor WM, Lim S, Huang M, et al. (2015). Immune history profoundly affects broadly protective B cell responses to influenza. Sci Transl Med 7, 316ra192–316ra192.

Baumgarth N (2013). How specific is too specific? B-cell responses to viral infections reveal the importance of breadth over depth. Immunol Rev 255, 82–94. [PubMed: 23947349]

Beasley DWC, and Barrett ADT (2002). Identification of Neutralizing Epitopes within Structural Domain III of the West Nile Virus Envelope Protein. Journal of Virology 76, 13097–13100. [PubMed: 12438639]

Bhattacharya D, Cheah MT, Franco CB, Hosen N, Pin CL, Sha WC, and Weissman IL (2007). Transcriptional profiling of antigen-dependent murine B cell differentiation and memory formation. J Immunol 179, 6808–6819. [PubMed: 17982071]

Castro CD, Ohta Y, Dooley H, and Flajnik MF (2013). Noncoordinate expression of J-chain and Blimp-1 define nurse shark plasma cell populations during ontogeny. European Journal of Immunology 43, 3061–3075. [PubMed: 23897025]

Cui Y, Chen X, Luo H, Fan Z, Luo J, He S, Yue H, Zhang P, and Chen R (2016). BioCircos.js: an interactive Circos JavaScript library for biological data visualization on web applications. Bioinformatics 32, 1740–1742. [PubMed: 26819473]

Dal Porto JM, Haberman AM, Kelsoe G, and Shlomchik MJ (2002). Very low affinity B cells form germinal centers, become memory B cells, and participate in secondary immune responses when higher affinity competition is reduced. The Journal of experimental medicine 195, 1215–1221. [PubMed: 11994427]

Dal Porto JM, Haberman a.M., Shlomchik MJ, and Kelsoe G (1998). Antigen drives very low affinity B cells to become plasmacytes and enter germinal centers. Journal of immunology (Baltimore, Md. : 1950) 161, 5373–5381.

DeKosky BJ, Lungu OI, Park D, Johnson EL, Charab W, Chrysostomou C, Kuroda D, Ellington AD, Ippolito GC, Gray JJ, and Georgiou G (2016). Large-scale sequence and structural comparisons of human naive and antigen-experienced antibody repertoires. Proceedings of the National Academy of Sciences 113, E2636–E2645.

Di Niro R, Lee SJ, Vander Heiden JA, Elsner RA, Trivedi N, Bannock JM, Gupta NT, Kleinstein SH, Vigneault F, Gilbert TJ, et al. (2015). Salmonella Infection Drives Promiscuous B Cell Activation Followed by Extrafollicular Affinity Maturation. Immunity 43, 120–131. [PubMed: 26187411]

Dogan I, Bertocci B, Vilmont V, Delbos F, Mégret J, Storck S, Reynaud C-A, and Weill J-C (2009). Multiple layers of B cell memory with different effector functions. Nature immunology 10, 1292–1299. [PubMed: 19855380]

Dubischar-Kastner K, Eder S, Buerger V, Gartner-Woelfl G, Kaltenboeck A, Schuller E, Tauber E, and Klade C (2010). Long-term immunity and immune response to a booster dose following vaccination with the inactivated Japanese encephalitis vaccine IXIARO, IC51. Vaccine 28, 5197–5202. [PubMed: 20541581]

Author Manuscript Author Manuscript Author Manuscript Author Manuscript

Engels N, Konig LM, Heemann C, Lutz J, Tsubata T, Griep S, Schrader V, and Wienands J (2009). Recruitment of the cytoplasmic adaptor Grb2 to surface IgG and IgE provides antigen receptor-intrinsic costimulation to class-switched B cells. Nat Immunol 10, 1018–1025. [PubMed: 19668218]

Escolano A, Steichen JM, Dosenovic P, Kulp DW, Golijanin J, Sok D, Freund NT, Gitlin AD, Oliveira T, Araki T, et al. (2016). Sequential Immunization Elicits Broadly Neutralizing Anti-HIV-1 Antibodies in Ig Knockin Mice. Cell 166, 1445–1458.e1412. [PubMed: 27610569]

Ferlenghi I, Clarke M, Ruttan T, Allison SL, Schalich J, Heinz FX, Harrison SC, Rey FA, and Fuller SD (2001). Molecular Organization of a Recombinant Subviral Particle from Tick-Borne Encephalitis Virus. Molecular Cell 7, 593–602. [PubMed: 11463384]

Fernandez E, Kose N, Edeling MA, Adhikari J, Sapparapu G, Lazarte SM, Nelson CA, Govero J, Gross ML, Fremont DH, et al. (2018). Mouse and Human Monoclonal Antibodies Protect against Infection by Multiple Genotypes of Japanese Encephalitis Virus. mBio 9, e00008–00018. [PubMed: 29487230]

Frei JC, Wirchnianski AS, Govero J, Vergnolle O, Dowd KA, Pierson TC, Kielian M, Girvin ME, Diamond MS, and Lai JR (2018). Engineered Dengue Virus Domain III Proteins Elicit Cross-Neutralizing Antibody Responses in Mice. Journal of virology 92, e01023–01018. [PubMed: 29976679]

Gitlin AD, Shulman Z, and Nussenzweig MC (2014). Clonal selection in the germinal centre by regulated proliferation and hypermutation. Nature 509, 637–640. [PubMed: 24805232]

Gitlin AD, von Boehmer L, Gazumyan A, Shulman Z, Oliveira TY, and Nussenzweig MC (2016). Independent Roles of Switching and Hypermutation in the Development and Persistence of B Lymphocyte Memory. Immunity.

Goodnow CC, Crosbie J, Adelstein S, Lavoie TB, Smith-Gill SJ, Brink RA, Pritchard-Briscoe H, Wotherspoon JS, Loblay RH, Raphael K, and et al. (1988). Altered immunoglobulin expression and functional silencing of self-reactive B lymphocytes in transgenic mice. Nature 334, 676–682. [PubMed: 3261841]

Guzman MG, Alvarez M, and Halstead SB (2013). Secondary infection as a risk factor for dengue hemorrhagic fever/dengue shock syndrome: an historical perspective and role of antibody-dependent enhancement of infection. Arch Virol 158, 1445–1459. [PubMed: 23471635]

Halstead SB (2017). Dengvaxia sensitizes seronegatives to vaccine enhanced disease regardless of age. Vaccine 35, 6355–6358. [PubMed: 29029938]

Halstead SB, Rojanasuphot S, and Sangkawibha N (1983). Original antigenic sin in dengue. The American journal of tropical medicine and hygiene 32, 154–156. [PubMed: 6824120]

Hardy RR, Carmack CE, Shinton SA, Kemp JD, and Hayakawa K (1991). Resolution and characterization of pro-B and pre-pro-B cell stages in normal mouse bone marrow. J Exp Med 173, 1213–1225. [PubMed: 1827140]

Havenar-Daughton C, Carnathan DG, Boopathy AV, Upadhyay AA, Murrell B, Reiss SM, Enemuo CA, Gebru EH, Choe Y, Dhadvai P, et al. (2019). Rapid Germinal Center and Antibody Responses in Non-human Primates after a Single Nanoparticle Vaccine Immunization. Cell Reports 29, 1756–1766.e1758. [PubMed: 31722194]

Ho IY, Bunker JJ, Erickson SA, Neu KE, Huang M, Cortese M, Pulendran B, and Wilson PC (2016). Refined protocol for generating monoclonal antibodies from single human and murine B cells. Journal of immunological methods 438, 67–70. [PubMed: 27600311]

Horikawa K, Martin SW, Pogue SL, Silver K, Peng K, Takatsu K, and Goodnow CC (2007). Enhancement and suppression of signaling by the conserved tail of IgG memory-type B cell antigen receptors. J Exp Med 204, 759–769. [PubMed: 17420266]

Ise W, Fujii K, Shiroguchi K, Ito A, Kometani K, Takeda K, Kawakami E, Yamashita K, Suzuki K, Okada T, and Kurosaki T (2018). T Follicular Helper Cell-Germinal Center B Cell Interaction Strength Regulates Entry into Plasma Cell or Recycling Germinal Center Cell Fate. Immunity 48, 702–715.e704. [PubMed: 29669250]

Jagger BW, Dowd KA, Chen RE, Desai P, Foreman B, Burgomaster KE, Himansu S, Kong W-P, Graham BS, Pierson TC, and Diamond MS (2019). Protective Efficacy of Nucleic Acid Vaccines

Author Manuscript Author Manuscript Author Manuscript Author Manuscript

Against Transmission of Zika Virus During Pregnancy in Mice. The Journal of Infectious Diseases 220, 1577–1588. [PubMed: 31260518]

Jash A, Wang Y, Weisel FJ, Scharer CD, Boss JM, Shlomchik MJ, and Bhattacharya D (2016). ZBTB32 Restricts the Duration of Memory B Cell Recall Responses. J Immunol 197, 1159–1168. [PubMed: 27357154]

Khalil AM, Cambier JC, and Shlomchik MJ (2012). B cell receptor signal transduction in the GC is short-circuited by high phosphatase activity. Science (New York, N.Y.) 336, 1178–1181.

Kometani K, Nakagawa R, Shinnakasu R, Kaji T, Rybouchkin A, Moriyama S, Furukawa K, Koseki H, Takemori T, and Kurosaki T (2013). Repression of the Transcription Factor Bach2 Contributes to Predisposition of IgG1 Memory B Cells toward Plasma Cell Differentiation. Immunity 39, 136–147. [PubMed: 23850379]

Kräutler NJ, Suan D, Butt D, Bourne K, Hermes JR, Chan TD, Sundling C, Kaplan W, Schofield P, Jackson J, et al. (2017). Differentiation of germinal center B cells into plasma cells is initiated by high-affinity antigen and completed by Tfh cells. The Journal of experimental medicine 214, 1259–1267. [PubMed: 28363897]

Krishnamurty AT, Thouvenel CD, Portugal S, Keitany GJ, Kim KS, Holder A, Crompton PD, Rawlings DJ, and Pepper M (2016). Somatically Hypermutated Plasmodium-Specific IgM(+) Memory B Cells Are Rapid, Plastic, Early Responders upon Malaria Rechallenge. Immunity 45, 402–414. [PubMed: 27473412]

Laidlaw BJ, Schmidt TH, Green JA, Allen CD, Okada T, and Cyster JG (2017). The Eph-related tyrosine kinase ligand Ephrin-B1 marks germinal center and memory precursor B cells. J Exp Med 214, 639–649. [PubMed: 28143955]

Lam WY, Jash A, Yao C, D'Souza L, Wong R, Nunley RM, Meares GP, Patti GJ, and Bhattacharya D (2018). Metabolic and Transcriptional Modules Independently Diversify Plasma Cell Lifespan and Function. Cell Rep in press.

Lanciotti RS, Roehrig JT, Deubel V, Smith J, Parker M, Steele K, Crise B, Volpe KE, Crabtree MB, Scherret JH, et al. (1999). Origin of the West Nile Virus Responsible for an Outbreak of Encephalitis in the Northeastern United States. Science 286, 2333. [PubMed: 10600742]

Lavinder JJ, Wine Y, Giesecke C, Ippolito GC, Horton AP, Lungu OI, Hoi KH, DeKosky BJ, Murrin EM, Wirth MM, et al. (2014). Identification and characterization of the constituent human serum antibodies elicited by vaccination. Proceedings of the National Academy of Sciences 111, 2259–2264.

Lefranc MP, Giudicelli V, Ginestoux C, Jabado-Michaloud J, Folch G, Bellahcene F, Wu Y, Gemrot E, Brochet X, Lane J, et al. (2009). IMGT, the international ImMunoGeneTics information system. Nucleic Acids Res 37, D1006–1012. [PubMed: 18978023]

Liao HX, Lynch R, Zhou T, Gao F, Alam SM, Boyd SD, Fire AZ, Roskin KM, Schramm CA, Zhang Z, et al. (2013). Co-evolution of a broadly neutralizing HIV-1 antibody and founder virus. Nature 496, 469–476. [PubMed: 23552890]

Luca VC, AbiMansour J, Nelson CA, and Fremont DH (2012). Crystal structure of the Japanese encephalitis virus envelope protein. Journal of virology 86, 2337–2346. [PubMed: 22156523]

Makhluf H, Buck MD, King K, Perry ST, Henn MR, and Shresta S (2013). Tracking the evolution of dengue virus strains D2S10 and D2S20 by 454 pyrosequencing. PloS one 8, e54220–e54220. [PubMed: 23342105]

Manz RA, Löhning M, Cassese G, Thiel A, and Radbruch A (1998). Survival of long-lived plasma cells is independent of antigen. International Immunology 10, 1703–1711. [PubMed: 9846699]

Martinez RJ, Andargachew R, Martinez HA, and Evavold BD (2016). Low-affinity CD4+ T cells are major responders in the primary immune response. Nature Communications 7, 13848.

McHeyzer-Williams LJ, Milpied PJ, Okitsu SL, and McHeyzer-Williams MG (2015). Class-switched memory B cells remodel BCRs within secondary germinal centers. Nature Immunology 16, 296–305. [PubMed: 25642821]

McNearney T, Hornickova Z, Markham R, Birdwell A, Arens M, Saah A, and Ratner L (1992). Relationship of human immunodeficiency virus type 1 sequence heterogeneity to stage of disease. Proc Natl Acad Sci U S A 89, 10247–10251. [PubMed: 1438212]

Author Manuscript Author Manuscript Author Manuscript Author Manuscript

Mukhopadhyay S, Kim B-S, Chipman PR, Rossmann MG, and Kuhn RJ (2003). Structure of West Nile Virus. Science 302, 248–248. [PubMed: 14551429]

Muramatsu M, Kinoshita K, Fagarasan S, Yamada S, Shinkai Y, and Honjo T (2000). Class switch recombination and hypermutation require activation-induced cytidine deaminase (AID), a potential RNA editing enzyme. Cell 102, 553–563. [PubMed: 11007474]

Nemazee DA, and Burki K (1989). Clonal deletion of B lymphocytes in a transgenic mouse bearing anti-MHC class I antibody genes. Nature 337, 562–566. [PubMed: 2783762]

Nybakken GE, Oliphant T, Johnson S, Burke S, Diamond MS, and Fremont DH (2005). Structural basis of West Nile virus neutralization by a therapeutic antibody. Nature 437, 764–769. [PubMed: 16193056]

Oliphant T, Engle M, Nybakken GE, Doane C, Johnson S, Huang L, Gorlatov S, Mehlhop E, Marri A, Chung KM, et al. (2005). Development of a humanized monoclonal antibody with therapeutic potential against West Nile virus. Nat Med 11, 522–530. [PubMed: 15852016]

Oliphant T, Nybakken GE, Austin SK, Xu Q, Bramson J, Loeb M, Throsby M, Fremont DH, Pierson TC, and Diamond MS (2007). Induction of epitope-specific neutralizing antibodies against West Nile virus. Journal of virology 81, 11828–11839. [PubMed: 17715236]

Pape KA, Maul RW, Dileepan T, Paustian AS, Gearhart PJ, and Jenkins MK (2018). Naive B Cells with High-Avidity Germline-Encoded Antigen Receptors Produce Persistent IgM(+) and Transient IgG(+) Memory B Cells. Immunity 48, 1135–1143 e1134. [PubMed: 29884459]

Pape KA, Taylor JJ, Maul RW, Gearhart PJ, and Jenkins MK (2011). Different B cell populations mediate early and late memory during an endogenous immune response. Science (New York, N.Y.) 331, 1203–1207.

Paus D, Phan TG, Chan TD, Gardam S, Basten A, and Brink R (2006). Antigen recognition strength regulates the choice between extrafollicular plasma cell and germinal center B cell differentiation. J Exp Med 203, 1081–1091. [PubMed: 16606676]

Pauthner M, Havenar-Daughton C, Sok D, Nkolola JP, Bastidas R, Boopathy AV, Carnathan DG, Chandrashekar A, Cirelli KM, Cottrell CA, et al. (2017). Elicitation of Robust Tier 2 Neutralizing Antibody Responses in Nonhuman Primates by HIV Envelope Trimer Immunization Using Optimized Approaches. Immunity 46, 1073–1088.e1076. [PubMed: 28636956]

Pelletier N, McHeyzer-Williams LJ, Wong KA, Urich E, Fazilleau N, and McHeyzer-Williams MG (2010). Plasma cells negatively regulate the follicular helper T cell program. Nature immunology 11, 1110–1118. [PubMed: 21037578]

Phan TG, Paus D, Chan TD, Turner ML, Nutt SL, Basten A, and Brink R (2006). High affinity germinal center B cells are actively selected into the plasma cell compartment. The Journal of experimental medicine 203, 2419–2424. [PubMed: 17030950]

Polo JM, Ci W, Licht JD, and Melnick A (2008). Reversible disruption of BCL6 repression complexes by CD40 signaling in normal and malignant B cells. Blood 112, 644–651. [PubMed: 18487509]

Purtha WE, Tedder TF, Johnson S, Bhattacharya D, and Diamond MS (2011). Memory B cells, but not long-lived plasma cells, possess antigen specificities for viral escape mutants. Journal of Experimental Medicine 208, 2599–2606. [PubMed: 22162833]

Radic MZ, Erikson J, Litwin S, and Weigert M (1993). B lymphocytes may escape tolerance by revising their antigen receptors. J Exp Med 177, 1165–1173. [PubMed: 8459210]

Richner JM, Himansu S, Dowd KA, Butler SL, Salazar V, Fox JM, Julander JG, Tang WW, Shresta S, Pierson TC, et al. (2017). Modified mRNA Vaccines Protect against Zika Virus Infection. Cell 168, 1114–1125.e1110. [PubMed: 28222903]

Ridderstad A, and Tarlinton DM (1998). Kinetics of establishing the memory B cell population as revealed by CD38 expression. J Immunol 160, 4688–4695. [PubMed: 9590214]

Robbiani DF, Bozzacco L, Keeffe JR, Khouri R, Olsen PC, Gazumyan A, Schaefer-Babajew D, Avila-Rios S, Nogueira L, Patel R, et al. (2017). Recurrent Potent Human Neutralizing Antibodies to Zika Virus in Brazil and Mexico. Cell 169, 597–609.e511. [PubMed: 28475892]

Roco JA, Mesin L, Binder SC, Nefzger C, Gonzalez-Figueroa P, Canete PF, Ellyard J, Shen Q, Robert PA, Cappello J, et al. (2019). Class-Switch Recombination Occurs Infrequently in Germinal Centers. Immunity 51, 337–350.e337. [PubMed: 31375460]

Author Manuscript Author Manuscript Author Manuscript Author Manuscript

Sabin AB (1952). Research on dengue during World War II. The American journal of tropical medicine and hygiene 1, 30–50. [PubMed: 14903434]

Sangkawibha N, Rojanasuphot S, Ahandrik S, Viriyapongse S, Jatanasen S, Salitul V, Phanthumachinda B, and Halstead SB (1984). Risk factors in dengue shock syndrome: a prospective epidemiologic study in Rayong, Thailand. I. The 1980 outbreak. Am J Epidemiol 120, 653–669. [PubMed: 6496446]

Sapparapu G, Fernandez E, Kose N, Bin C, Fox JM, Bombardi RG, Zhao H, Nelson CA, Bryan AL, Barnes T, et al. (2016). Neutralizing human antibodies prevent Zika virus replication and fetal disease in mice. Nature 540, 443–447. [PubMed: 27819683]

Scheid JF, Mouquet H, Kofer J, Yurasov S, Nussenzweig MC, and Wardemann H (2011). Differential regulation of self-reactivity discriminates between IgG+ human circulating memory B cells and bone marrow plasma cells. Proceedings of the National Academy of Sciences of the United States of America 108, 18044–18048. [PubMed: 22025722]

Seifert M, Przekopowitz M, Taudien S, Lollies A, Ronge V, Drees B, Lindemann M, Hillen U, Engler H, Singer BB, and Kuppers R (2015). Functional capacities of human IgM memory B cells in early inflammatory responses and secondary germinal center reactions. Proc Natl Acad Sci U S A 112, E546–555. [PubMed: 25624468]

Shen W-F, Galula JU, Liu J-H, Liao M-Y, Huang C-H, Wang Y-C, Wu H-C, Liang J-J, Lin Y-L, Whitney MT, et al. (2018). Epitope resurfacing on dengue virus-like particle vaccine preparation to induce broad neutralizing antibody. eLife 7, e38970. [PubMed: 30334522]

Shinnakasu R, Inoue T, Kometani K, Moriyama S, Adachi Y, Nakayama M, Takahashi Y, Fukuyama H, Okada T, and Kurosaki T (2016). Regulated selection of germinal-center cells into the memory B cell compartment. Nature Immunology advance on, 861–869.

Silver J, Zuo T, Chaudhary N, Kumari R, Tong P, Giguere S, Granato A, Donthula R, Devereaux C, and Wesemann DR (2018). Stochasticity enables BCR-independent germinal center initiation and antibody affinity maturation. The Journal of experimental medicine 215, 77. [PubMed: 29247044]

Slifka MK, Antia R, Whitmire JK, and Ahmed R (1998). Humoral immunity due to long-lived plasma cells. Immunity 8, 363–372. [PubMed: 9529153]

Slon-Campos JL, Dejnirattisai W, Jagger BW, López-Camacho C, Wongwiwat W, Durnell LA, Winkler ES, Chen RE, Reyes-Sandoval A, Rey FA, et al. (2019). A protective Zika virus E-dimer-based subunit vaccine engineered to abrogate antibody-dependent enhancement of dengue infection. Nature Immunology 20, 1291–1298. [PubMed: 31477918]

Smith K, Garman L, Wrammert J, Zheng N-Y, Capra JD, Ahmed R, and Wilson PC (2009). Rapid generation of fully human monoclonal antibodies specific to a vaccinating antigen. Nat Protoc 4, 372–384. [PubMed: 19247287]

Smith KGC, Light A, Nossal GJV, and Tarlinton DM (1997). The extent of affinity maturation differs between the memory and antibody-forming cell compartments in the primary immune response. EMBO Journal 16, 2996–3006. [PubMed: 9214617]

Song B-H, Yun G-N, Kim J-K, Yun S-I, and Lee Y-M (2012). Biological and genetic properties of SA14-14-2, a live-attenuated Japanese encephalitis vaccine that is currently available for humans. Journal of Microbiology 50, 698–706.

Stuart T, Butler A, Hoffman P, Hafemeister C, Papalexi E, Mauck WM III, Hao Y, Stoeckius M, Smibert P, and Satija R (2019). Comprehensive Integration of Single-Cell Data. Cell 177, 1888–1902.e1821. [PubMed: 31178118]

Suan D, Kräutler NJ, Maag JLV, Butt D, Bourne K, Hermes JR, Avery DT, Young C, Statham A, Elliott M, et al. (2017). CCR6 Defines Memory B Cell Precursors in Mouse and Human Germinal Centers, Revealing Light-Zone Location and Predominant Low Antigen Affinity. Immunity 47, 1142–1153.e1144. [PubMed: 29262350]

Tarlinton D (2006). B-cell memory: are subsets necessary? Nat Rev Immunol 6, 785–790. [PubMed: 16998511]

Taylor JJ, Pape KA, and Jenkins MK (2012). A germinal center-independent pathway generates unswitched memory B cells early in the primary response. The Journal of experimental medicine 209, 597–606. [PubMed: 22370719]

Author Manuscript Author Manuscript Author Manuscript Author Manuscript

Taylor JJ, Pape KA, Steach HR, and Jenkins MK (2015). Humoral immunity. Apoptosis and antigen affinity limit effector cell differentiation of a single naive B cell. Science 347, 784–787. [PubMed: 25636798]

Tiegs SL, Russell DM, and Nemazee D (1993). Receptor editing in self-reactive bone marrow B cells. J Exp Med 177, 1009–1020. [PubMed: 8459201]

Tiller T, Busse CE, and Wardemann H (2009). Cloning and expression of murine Ig genes from single B cells. J Immunol Methods 350, 183–193. [PubMed: 19716372]

Tiller T, Meffre E, Yurasov S, Tsuiji M, Nussenzweig MC, and Wardemann H (2008). Efficient generation of monoclonal antibodies from single human B cells by single cell RT-PCR and expression vector cloning. Journal of Immunological Methods 329, 112–124. [PubMed: 17996249]

Tiller T, Tsuiji M, Yurasov S, Velinzon K, Nussenzweig MC, and Wardemann H (2007). Autoreactivity in human IgG+ memory B cells. Immunity 26, 205–213. [PubMed: 17306569]

Tomayko MM, Anderson SM, Brayton CE, Sadanand S, Steinel NC, Behrens TW, and Shlomchik MJ (2008). Systematic comparison of gene expression between murine memory and naive B cells demonstrates that memory B cells have unique signaling capabilities. Journal of immunology (Baltimore, Md. : 1950) 181, 27–38.

Tomayko MM, Steinel NC, Anderson SM, and Shlomchik MJ (2010). Cutting Edge: Hierarchy of Maturity of Murine Memory B Cell Subsets. The Journal of Immunology 185, 7146. [PubMed: 21078902]

Waisman A, Kraus M, Seagal J, Ghosh S, Melamed D, Song J, Sasaki Y, Classen S, Lutz C, Brombacher F, et al. (2007). IgG1 B cell receptor signaling is inhibited by CD22 and promotes the development of B cells whose survival is less dependent on Ig alpha/beta. J Exp Med 204, 747–758. [PubMed: 17420268]

Wan Z, Chen X, Chen H, Ji Q, Chen Y, Wang J, Cao Y, Wang F, Lou J, Tang Z, and Liu W (2015). The activation of IgM- or isotype-switched IgG- and IgE-BCR exhibits distinct mechanical force sensitivity and threshold. eLife 4, e06925.

Wang Y, Shi J, Yan J, Xiao Z, Hou X, Lu P, Hou S, Mao T, Liu W, Ma Y, et al. (2017). Germinal-center development of memory B cells driven by IL-9 from follicular helper T cells. Nature Immunology 18, 921. [PubMed: 28650481]

Weisel FJ, Zuccarino-Catania GV, Chikina M, and Shlomchik MJ (2016). A Temporal Switch in the Germinal Center Determines Differential Output of Memory B and Plasma Cells. Immunity 44, 116–130. [PubMed: 26795247]

Wolock SL, Lopez R, and Klein AM (2019). Scrublet: Computational Identification of Cell Doublets in Single-Cell Transcriptomic Data. Cell Syst 8, 281–291.e289. [PubMed: 30954476]

Wong R, and Bhattacharya D (2019). Basics of memory B-cell responses: lessons from and for the real world. Immunology 156, 120–129. [PubMed: 30488482]

Wu X, Zhou T, Zhu J, Zhang B, Georgiev I, Wang C, Chen X, Longo NS, Louder M, McKee K, et al. (2011). Focused evolution of HIV-1 neutralizing antibodies revealed by structures and deep sequencing. Science 333, 1593–1602. [PubMed: 21835983]

Zaretsky I, Atrakchi O, Mazor RD, Stoler-Barak L, Biram A, Feigelson SW, Gitlin AD, Engelhardt B, and Shulman Z (2017). ICAMs support B cell interactions with T follicular helper cells and promote clonal selection. J Exp Med 214, 3435–3448. [PubMed: 28939548]

Zhang J, Kobert K, Flouri T, and Stamatakis A (2014). PEAR: a fast and accurate Illumina Paired-End reAd mergeR. Bioinformatics 30, 614–620. [PubMed: 24142950]

Zhang R, Miner JJ, Gorman MJ, Rausch K, Ramage H, White JP, Zuiani A, Zhang P, Fernandez E, Zhang Q, et al. (2016). A CRISPR screen defines a signal peptide processing pathway required by flaviviruses. Nature 535, 164. [PubMed: 27383988]

Zhao H, Fernandez E, Dowd KA, Speer SD, Platt DJ, Gorman MJ, Govero J, Nelson CA, Pierson TC, Diamond MS, and Fremont DH (2016). Structural Basis of Zika Virus-Specific Antibody Protection. Cell 166, 1016–1027. [PubMed: 27475895]

Zhao H, Xu L, Bombardi R, Nargi R, Deng Z, Errico JM, Nelson CA, Dowd KA, Pierson TC, Crowe JE Jr., et al. (2019). Mechanism of differential Zika and dengue virus neutralization by a public antibody lineage targeting the DIII lateral ridge. J Exp Med.

Author Manuscript Author Manuscript Author Manuscript Author Manuscript

Zuccarino-Catania GV, Sadanand S, Weisel FJ, Tomayko MM, Meng H, Kleinstein SH, Good-Jacobson KL, and Shlomchik MJ (2014). CD80 and PD-L2 define functionally distinct memory B cell subsets that are independent of antibody isotype. Nat Immunol 15, 631–637. [PubMed: 24880458]

Author Manuscript Author Manuscript Author Manuscript Author Manuscript

Highlights:

- Flavivirus-specific memory B cells bypass germinal centers in recall responses
- Recall responses are restricted by the starting clonal diversity of memory B cells
- Low germline affinity cells enter the germinal center to promote memory diversity
- Memory B cell precursor germline affinity is lower than of long-lived plasma cells

Author Manuscript Author Manuscript Author Manuscript Author Manuscript

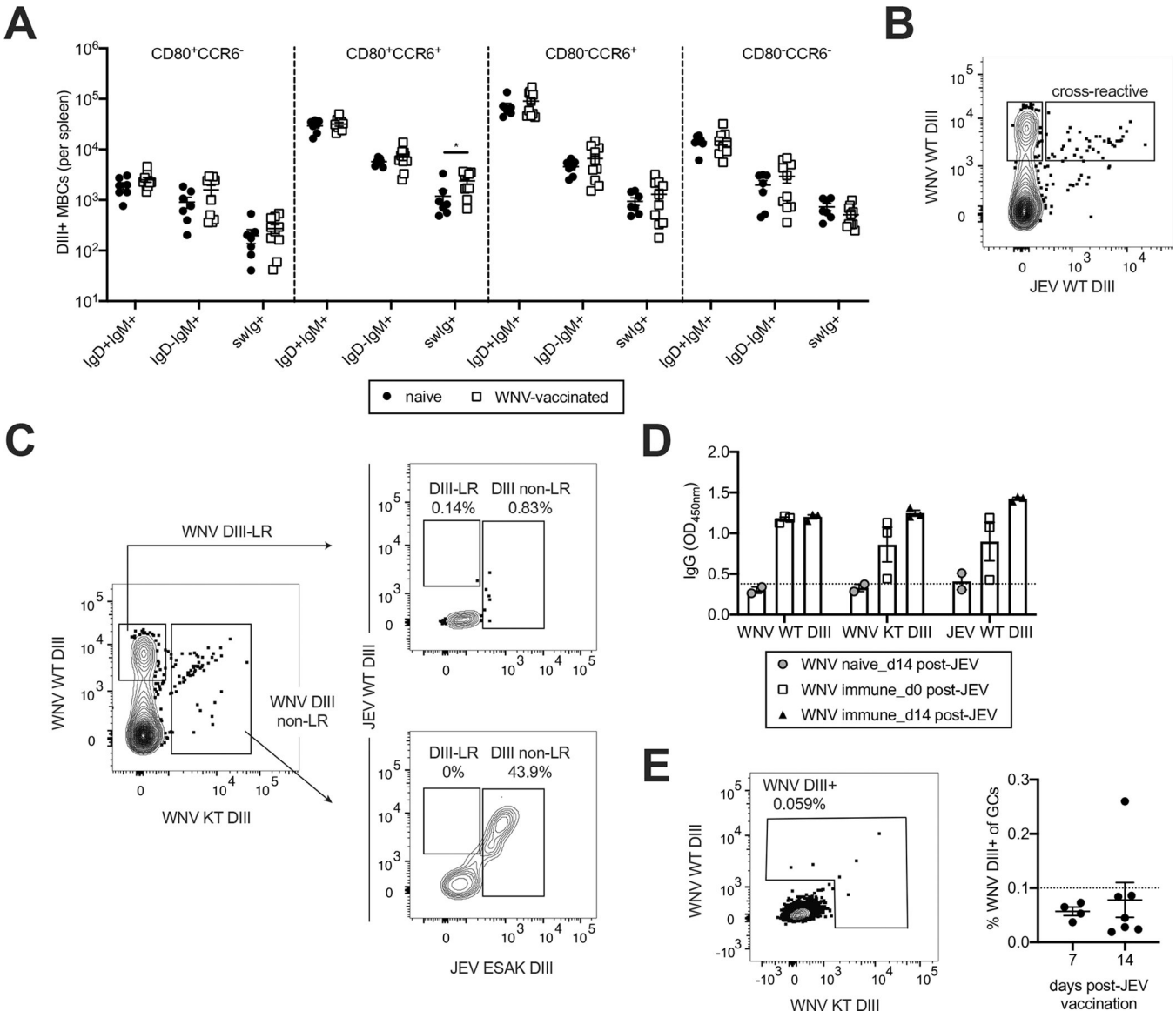

Figure 1. Plasma cell-biased MBCs recognize and respond to heterologous antigens.

(**A**) Mice were vaccinated with inactivated WNV vaccine and the number of DIII-specific cells in different MBC subsets was calculated by flow cytometry 8–12 weeks later. WNV-vaccinated mice are compared to naïve animals. Mean ± SEM are shown; each symbol represents an individual mouse. Data are pooled from two independent experiments. *$p < 0.05$; student's two-tailed t test for each subset. (**B**) Representative flow cytometry plot showing cross-reactivity between WNV DIII- and JEV DIII-specific swIg CD80$^+$ MBCs. WNV DIII-binding cells were enriched from 5 pooled spleens from WNV-vaccinated mice and then stained for JEV DIII specificity. (**C**) Representative flow cytometry plots showing the cross-reactivity of WNV DIII-LR and WNV DIII non-LR cells to JEV DIII-LR and JEV DIII non-LR cells. Cells originate from the same experiment as in (**B**). (**D**) Sera from naïve and WNV-immune mice were assessed for WNV WT, WNV KT DIII, and JEV WT DIII binding before (D0) and 14 days post JEV vaccination. OD450nm values at a 1:50 serum

Author Manuscript Author Manuscript Author Manuscript Author Manuscript

dilution is shown. Mean ± SEM are shown; each symbol represents an individual mouse. Data comes from one experiment. (**E**) The frequency of WNV DIII-specific GC B cells ($CD19^{+}GL7^{+}IgD^{-}CD38^{-}$) 7 and 14 days after JEV vaccination of WNV-vaccinated mice was quantified by flow cytometry. A representative plot of DIII-specific GC B cells is shown on the left and quantified on the right. Mean ± SEM are shown; each symbol represents an individual mouse. Data comes from one experiment. See also Figure S1.

Author Manuscript Author Manuscript Author Manuscript Author Manuscript

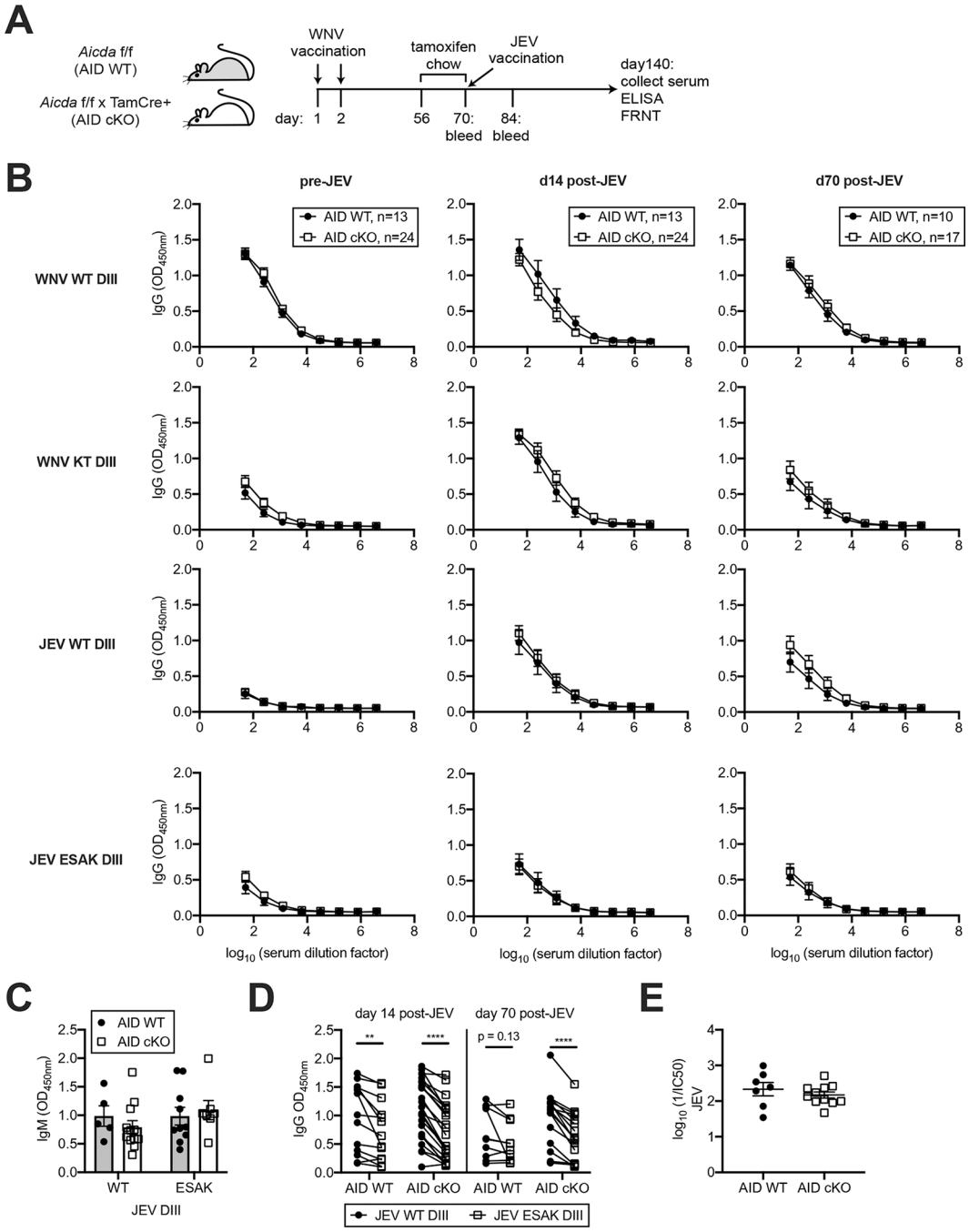

Figure 2. MBCs do not require additional affinity maturation to respond to heterologous flavivirus challenges.

(**A**) Schematic representation of the experimental setup for WNV vaccination and JEV recall responses. (**B**) Serum from WNV-immune *Aicda* f/f × TamCre (AID cKO) and *Aicda* f/f (AID WT) was collected before, 14, and 70 days after JEV vaccination. Serum binding curves against WNV WT DIII, WNV KT DIII, JEV WT DIII, and JEV ESAK DIII for each timepoint are shown. Mean ± SEM values are shown. Data are pooled from 3 independent experiments where 2–9 mice per genotype was used for each experiment. (**C**) Serum from

Author Manuscript Author Manuscript Author Manuscript Author Manuscript

WNV-immune AID WT and AID cKO mice was collected ten weeks after JEV vaccination. JEV WT and JEV ESAK DIII specific IgM levels are shown as the OD_{450nm} values from serum diluted 1:50. Each symbol represents an individual mouse. Mean ± SEM are shown. Data are pooled from two independent experiments. (**D**) IgG levels, shown as OD_{450nm} values for 1:50 diluted serum, collected in (B), for binding to JEV WT and JEV ESAK DIII. Each symbol connected by lines represents paired values from an individual mouse. Data are pooled from three independent experiments. (**E**) Neutralizing antibody titers (1/IC50) to JEV were measured by a focus reduction neutralization test (FRNT) from serum collected in (B). Mean ± SEM are shown; each symbol represents an individual mouse. See also Figures S2 and S3.

Author Manuscript Author Manuscript Author Manuscript Author Manuscript

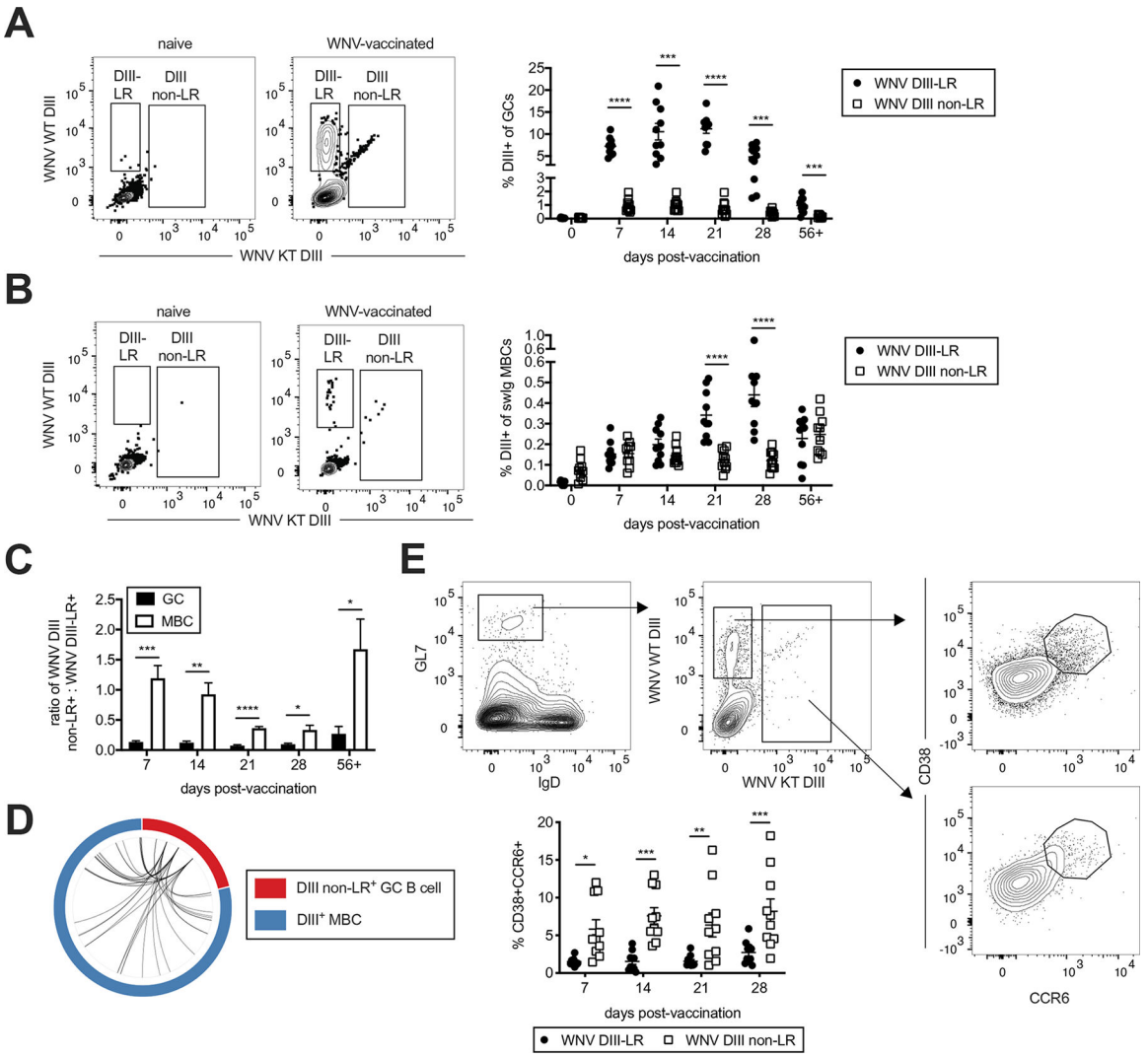

Figure 3. MBCs are actively selected from GC B cells.

(**A**) Mice were immunized with inactivated WNV vaccine and DIII-specificities in GCs ($CD19^+GL7^+IgD^-CD38^-$) were enumerated by flow cytometry at days 7, 14, 21, 28 and 56+. A representative plot of DIII-specific GC B cells is shown on the left and quantified on the right. Mean frequencies ± SEM are shown; each symbol represents an individual mouse. *** $p < 0.001$, **** $p < 0.0001$; paired student's t-test. Data are pooled from two independent experiments. (**B**) The frequencies of WNV DIII-LR and WNV DIII non-LR binders in swIg $CD80^+CCR6^+$ MBCs were quantified by flow cytometry at different timepoints after WNV vaccination. A representative plot of DIII-specific MBCs is shown on the left and quantified on the right. Mean values ± SEM are shown; each symbol represents an individual mouse. *** $p < 0.001$, **** $p < 0.0001$; paired student's t-test. Data are pooled from two independent experiments. (**C**) Ratios of WNV DIII non-LR to WNV DIII-LR specific cells were quantified for GC B cells and MBCs using values in (A) and (B). Mean values ± SEM are shown. *$p < 0.05$, ** $p < 0.01$, *** $p < 0.001$, **** $p < 0.0001$; paired student's t-test. **(D)** WNV DIII non-LR GC B cells and WNV $DIII^+$ MBCs were sorted two weeks after WNV vaccination of wild-type mice and IgG sequences amplified. Clonal

Author Manuscript Author Manuscript Author Manuscript Author Manuscript

overlap between the germline IgH sequences from these two populations are displayed as links in the BioCircos plot. (**E**) The frequency of $CD38^{+}CCR6^{+}$ expressing MBC precursor cells within WNV DIII-LR and WNV DIII non-LR specific GC B cells ($CD19^{+}GL7^{+}IgD^{-}$) was quantified by flow cytometry. The gating strategy is shown on the top with a representative CD38+CCR6+ gate shown for DIII-LR and DIII non-LR cells. Mean values ± SEM are shown; each symbol represents an individual mouse. Data are pooled from two independent experiments.

Author Manuscript Author Manuscript Author Manuscript Author Manuscript

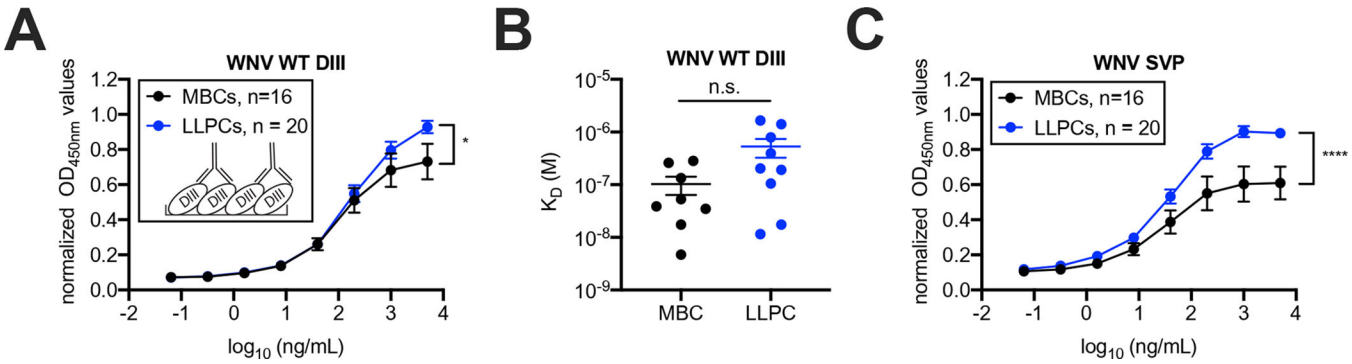

Figure 4. MBCs have lower avidity for their antigens than do LLPCs.

(**A**) Monoclonal Abs from WNV-immune mice were isolated from MBCs and LLPCs, and WNV DIII reactivity was confirmed by ELISA. MAb binding curves for WNV WT DIII were performed using ELISA. Mean ± SEM are shown. *p < 0.05; 2-way ANOVA. (**B**) Binding affinity ($K_{D,\ kinetic}$) to WNV WT DIII for a subset of mAbs was determined by biolayer interferometry. Mean ± SEM are shown; each symbol represents one mAbs. n.s. indicates p > 0.05; Mann-Whitney test. (**C**) MAb binding curves for WNV subviral particles (SVPs) were performed by ELISA. Mean ± SEM are shown. ****p < 0.0001; 2-way ANOVA. See also Figure S4.

Author Manuscript Author Manuscript Author Manuscript Author Manuscript

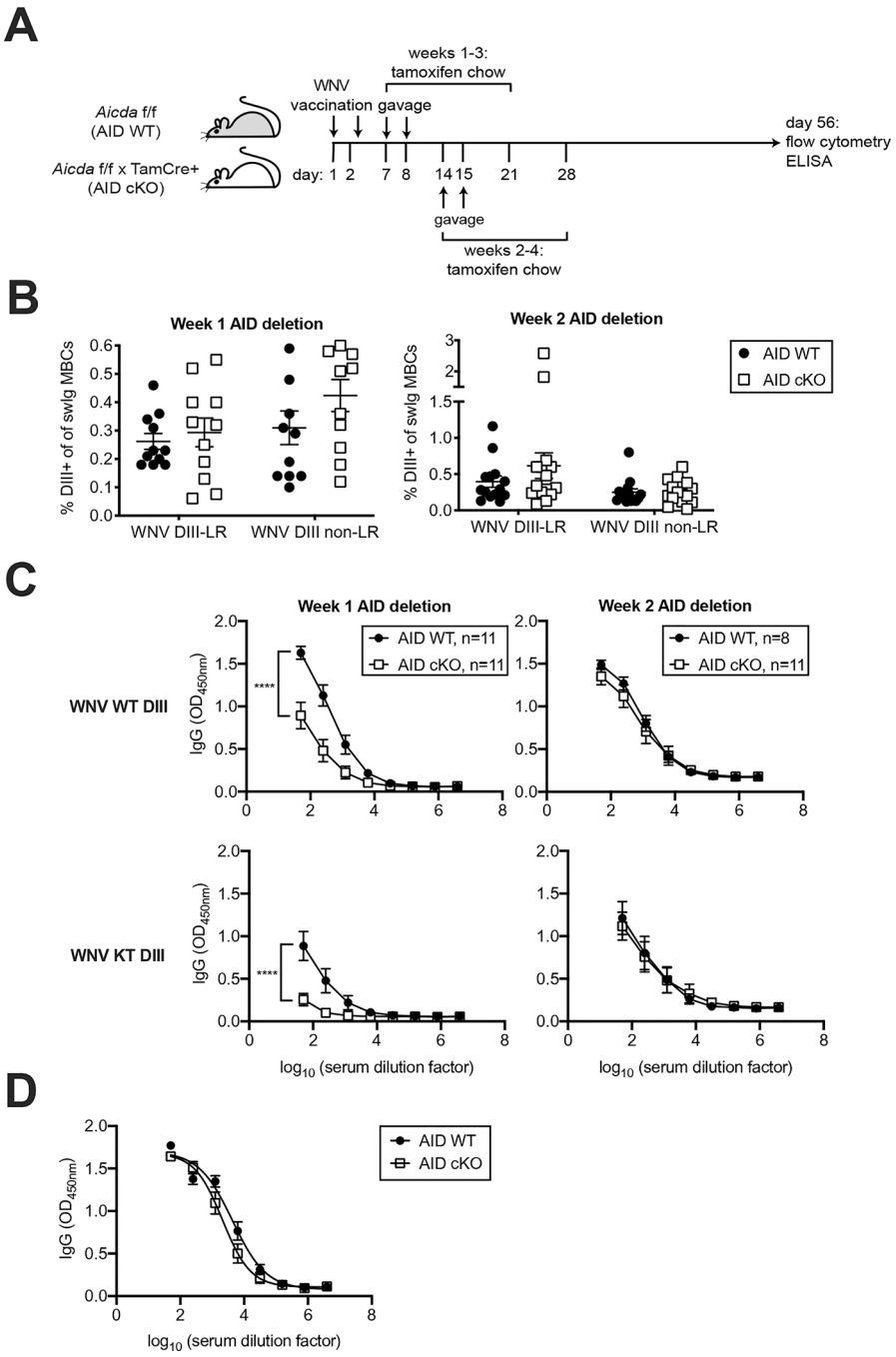

Figure 5. Absolute affinity thresholds do not segregate MBCs from LLPCs in vivo.

(**A**) Experimental setup to temporally ablate AID during ongoing GC reactions. (**B**) Frequencies of WNV DIII-LR and WNV DIII non-LR specific MBCs were quantified by flow cytometry for each AID genotype and deletion group. Mean values ± SEM are shown; each symbol represents an individual mouse. Data are pooled from two independent experiments. (**C**) Serum IgG antibody binding curves to WNV WT DIII and WNV KT DIII are shown for each AID deletion group. Mean values ± SEM are shown. Data are pooled from two independent experiments consisting of 4–7 mice per genotype for each

Author Manuscript Author Manuscript Author Manuscript Author Manuscript

experiment. ***$p < 0.001$ by 2-way ANOVA. (**D**) Serum from week 1 AID deletion was assessed for WNV SVP binding by ELISA. Mean values ± SEM are shown. See also Figure S5.

Author Manuscript Author Manuscript Author Manuscript Author Manuscript

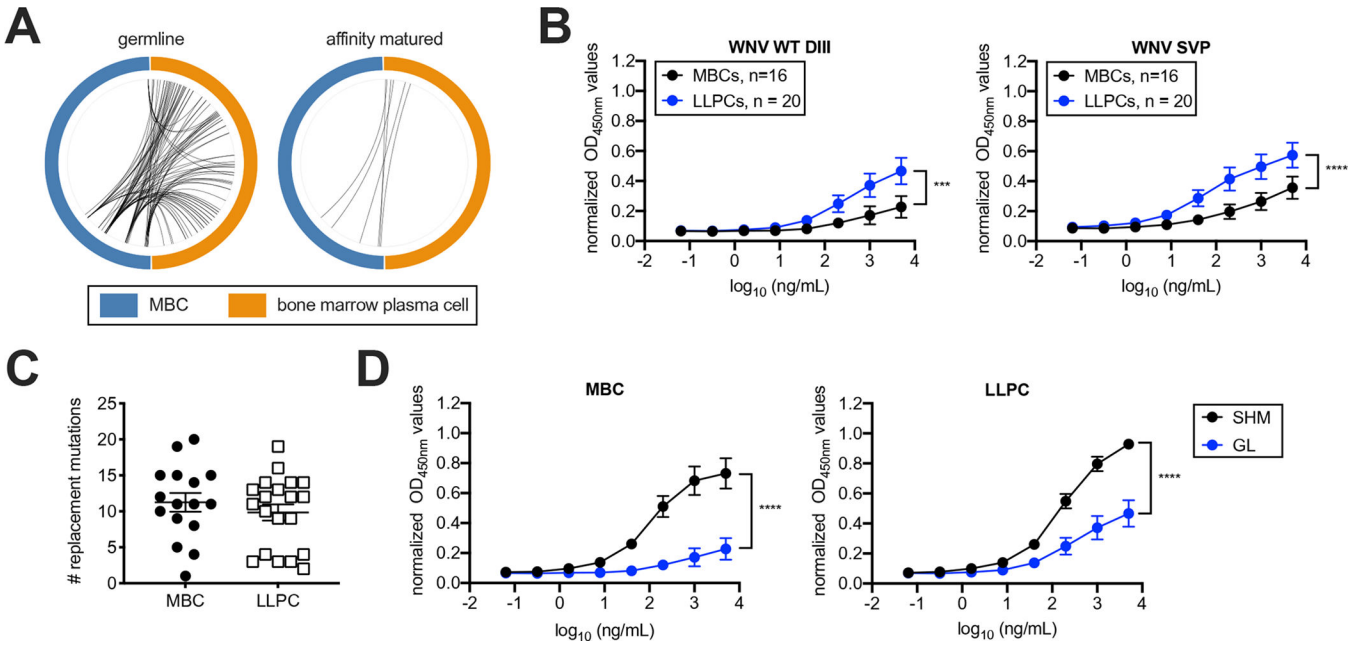

Figure 6. Germline affinities of MBC-derived antibodies are lower than those from LLPCs.

(**A**) BioCircos plots showing clonal overlap at the germline-reverted and affinity matured IgG sequence from sorted WNV DIII$^+$ BMPCs and WNV DIII$^+$ MBCs four weeks after WNV vaccination. Each link represents a shared clone between the two populations. (**B**) Monoclonal Abs isolated in Figure 4 were reverted to their germline sequences, and binding curves against monomeric WNV WT DIII and SVPs were measured by ELISA. Mean values ± SEM are shown. ***p < 0.001 and ****p < 0.0001; 2-way ANOVA. (**C**) The total number of replacement mutations in the heavy and light chains of the isolated mAbs are plotted. Mean ± SEM are shown; each symbol represents one mAb. (**D**) ELISA binding curves for monomeric WNV WT DIII are compared for germline-reverted and somatically-mutated mAbs from MBCs and LLPCs. Mean ± SEM are shown. ****p < 0.0001; two-way ANOVA. See also Figure S6.

Author Manuscript Author Manuscript Author Manuscript Author Manuscript

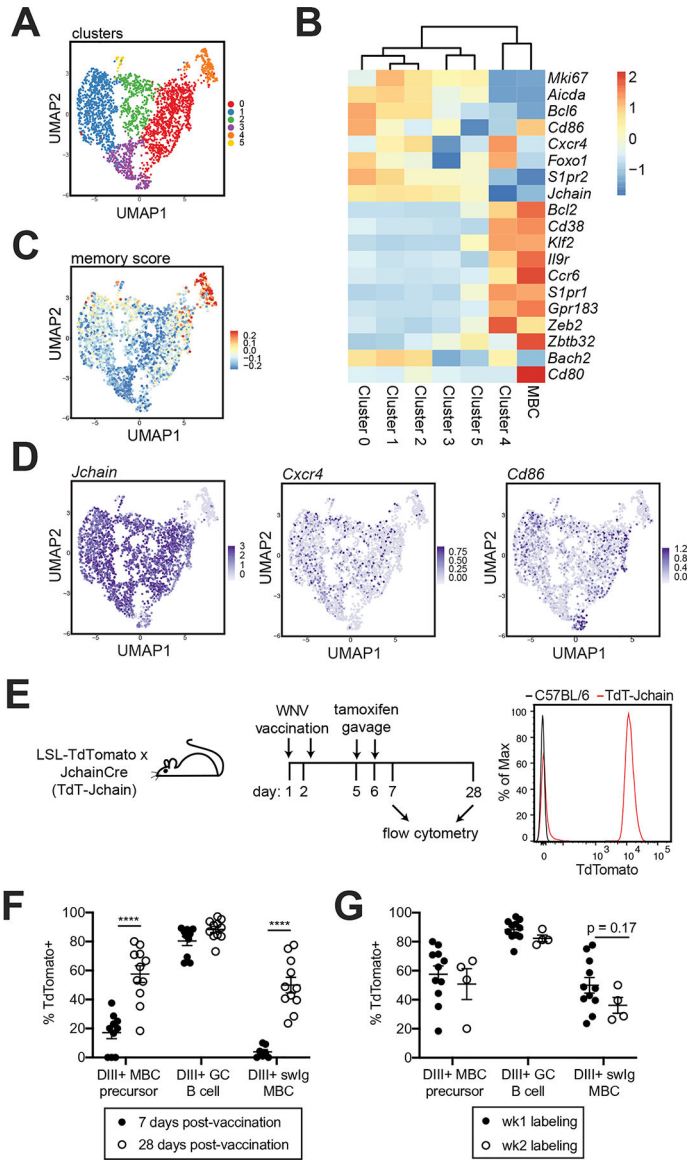

Figure 7. MBCs are continuously selected from GCs.

(**A**) DIII-specific GC B cells ($CD19^+GL7^+IgD^-EphrinB1^+$) were isolated one week after WNV vaccination, subjected to single cell RNA-sequencing and analyzed using Seurat. UMAP plot displaying cells colored by transcriptional color identity. (**B**) Heatmap of signature GC B cell and MBC genes for each cluster as well as sorted MBCs. Averages for all single cells in each cluster and all MBCs are shown. (**C**) UMAP plot showing cells and their MBC module score (*Klf2*, *Zbtb32*, *Bach2*, *Il9r*, *Ccr6*, *Cd38*, and *S1pr1*). (**D**) UMAP plot highlighting gene expression level per cell for *Jchain*, *Cxcr4* (dark zone), and *CD86* (light zone). (**E**) Schematic representation of GC lineage tracing experiment. A representative histogram for TdTomato expression in polyclonal MBC precursors ($CD19^+GL7^+IgD^-IgM^-CD38^+EfnB1^+$) is shown (right). (**F**) The frequency of TdTomato expression in the DIII+ and polyclonal MBC precursor, DIII+ GC B cells ($CD19^+GL7^+IgD^-CD38^-EfnB1^+$) and DIII+ swIg MBC populations is quantified by flow cytometry in TdT-

Author Manuscript Author Manuscript Author Manuscript Author Manuscript

Jchain mice labelled 5 and 6 days after WNV vaccination, and analyzed 1 or 22 days later. Mean ± SEM are shown. ****$p < 0.0001$; paired Student's t test for each population. (**G**) Frequency of TdTomato-labelled cells in TdT-Jchain mice treated with tamoxifen 14 and 15 days after WNV vaccination was analyzed by flow cytometry 13 days later (28 days after WNV vaccination) and compared to week 1 labeling. Week 1 labeling at 28 days after WNV vaccination are the same data as shown in (**F**). Student's t test was used for statistical analysis. See also Figure S7.

Author Manuscript Author Manuscript Author Manuscript Author Manuscript

KEY RESOURCES TABLE

REAGENT or RESOURCE	SOURCE	IDENTIFIER
Antibodies		
CD19 (clone 6D5) Alexa Fluor 700	Biolegend	Cat#115528; RRID: AB_493735
GL7 FITC	Biolegend	Cat#144604; RRID: AB_2561697
GL7 PerCP-Cy5.5	Biolegend	Cat#144610; RRID: AB_2562979
GL7 PE	Biolegend	Cat#144608; RRID: AB_2562926
GL7 Pacific Blue	Biolegend	Cat#144614; RRID: AB_2563292
CD38 (clone 90) BV510	BD biosciences	Cat#740129; RRID: AB_2739886
CD38 (clone 90) APC-Cy7	Biolegend	Cat#102728; RRID: AB_2616968
CD138 (clone 281–2) PE	Biolegend	Cat# 142504; RRID: AB_10916119
CD138 (clone 281–2) APC	Biolegend	Cat# 142506; RRID: AB_10962911
IgM (clone RMM-1) APC	Biolegend	Cat# 406509; RRID: AB_315059
IgD (clone 11–26c.2a) PerCP-Cy5.5	Biolegend	Cat# 405710; RRID: AB_1575113
IgD (clone 11–26c.2a) PE-Dazzle594	Biolegend	Cat# 405742; RRID: AB_2571985
IgD (clone 11–26c.2a) BV510	Biolegend	Cat# 405723; RRID: AB_2562742
IgD (clone 11–26c.2a) BV605	Biolegend	Cat# 405727; RRID: AB_2562887
CD80 (clone 16–10A1) PE	Biolegend	Cat#104708; RRID: AB_313129
CD80 (clone 16–10A1) Alexa Fluor 488	Biolegend	Cat#104716; RRID: AB_492822
CD80 (clone 16–10A1) BV510	Biolegend	Cat#104741; RRID: AB_2810337
PD-L2 (clone TY25) BV421	Biolegend	Cat#107219; RRID: AB_2728127
PD-L2 (clone TY25) PE-Dazzle594	Biolegend	Cat#107216; RRID: AB_2749894
CD73 (clone TY/11.8) APC-Fire750	Biolegend	Cat#127222; RRID: AB_2716101
CD23 (clone B3B4) BV510	Biolegend	Cat#101623; RRID: AB_2563705
B220 (clone RA3–6B2) FITC	Biolegend	Cat#103206; RRID: AB_312991
CCR6 (clone 29–2L17) PE-Cy7	Biolegend	Cat#129816; RRID: AB_2072798
IgM (clone II/41) PerCP-e710	eBioscience	Cat#46-5790-82; RRID: AB_1834435
CD21/35 (clone 4E3) FITC	eBioscience	Cat#11-0212-82; RRID: AB_464976
EphrinB1-biotin	R&D Systems	Cat#BAF473; RRID: AB_2293418
CD11b (clone M1/70)	Bio X Cell	Cat#BE0007; RRID: AB_1107582
CD3 (clone 2C11)	Bio X Cell	Cat#BE0001–1; RRID: AB_1107634
CD4 (clone GK1.5)	Bio X Cell	Cat#BE0003–1; RRID: AB_1107636
CD8 (clone 53–6.7)	Bio X Cell	Cat#BE0004–1; RRID: AB_1107671
Ter119	Bio X Cell	Cat# BE0183; RRID: AB_10949625
Humanized E16	BEI Resources	NR-31082
JEV-31	Fernandez et al, 2018	N/A

Author Manuscript Author Manuscript Author Manuscript Author Manuscript

REAGENT or RESOURCE	SOURCE	IDENTIFIER
Streptavidin BV421	Biolegend	Cat#405225
Streptavidin BV605	Biolegend	Cat#405229
Streptavidin BV711	Biolegend	Cat#40524
Streptavidin PE	Biolegend	Cat#405204
Streptavidin APC	Biolegend	Cat# 405207
Streptavidin HRP	BD Bioscience	Cat#554066
Streptavidin	Invitrogen	Cat#434302
Goat Anti-Rat IgG(H+L), Mouse ads-UNLB	SouthernBiotech	Cat#: 3050–01; RRID: AB_2795826
Goat Anti-Human Kappa, Mouse ads-UNLB	SouthernBiotech	Cat#: 2061–01; RRID: AB_2795728
Purified rat anti-mouse Ig, k Light Chain (clone 187.1)	BD Pharmigen	Cat#559749
Peroxidase AffiniPure Donkey Anti-Human IgG (H+L)	Jackson ImmunoResearch	Cat#709-035-149; RRID: AB_2340495
Biotin-SP (long spacer) AffiniPure Goat Anti-Mouse IgM, μ chain specific	Jackson ImmunoResearch	Cat#115-065-075; RRID: AB_2338566
Biotin-SP-AffiniPure Donkey Anti-Mouse IgG (H+L) (min X Bov,Ck,Gt,GP,Hms,Hrs,Hu,Rb,Rat,Shp Sr Prot)	Jackson ImmunoResearch	Cat#715-065-151; RRID: AB_2340785
mAID-2-biotin	eBioscience	Cat#13-5959-82; RRID: AB_2572798
Anti-ERK2 (clone C-14)	Santa Cruz Biotechnology	Cat# sc-154; RRID: AB_2141292
Bacterial and Virus Strains		
BL21(DE3) Competent E. coli	New England BioLabs	Cat#C2427
WNV-NY99	Lanciotti et al., 1999	N/A
JEV SA-14-14-2	Song, et al., 2012	N/A
DENV-2 D2S20	Makhluf, et al., 2013	N/A
ZIKV Dakar	Zhao et al., 2016	ZIKV Dakar strain 41519
XL-1 Blue Competent Cells	Agilent	Cat#200249
Chemicals, Peptides, and Recombinant Proteins		
ZIKV WT DIII	Zhao et al., 2016	N/A
ZIKV WT DIII-biotin	Zhao et al., 2016	N/A
ZIKV AT DIII	Zhao et al., 2016	N/A
ZIKV AT DIII-biotin	Zhao et al., 2016	N/A
Low IgG Fetal Bovine Serum	ThermoFisher Scientific	Cat#16250078
Tamoxifen-containing chow	Envigo	Cat#TD.130860
Corn oil	Millipore Sigma	Cat# C8267
Tamoxifen	MedChemExpress	Cat# HY-13757A
Alfa Aesar™ 3,3’,5,5’-Tetramethylbenzidine solution	Fisher Scientific	Cat#AAJ61325AU
GeneJuice transfection reagent	Millipore Sigma	Cat#70967
Pokeweed mitogen lectin	Sigma-Aldrich	Cat#L9379
Lipopolysaccharide	Sigma-Aldrich	Cat#L2630
Adult bovine serum	MP Biomedicals	Cat# 0219135290

Author Manuscript Author Manuscript Author Manuscript Author Manuscript

REAGENT or RESOURCE	SOURCE	IDENTIFIER
Bovine Serum Albumin	Sigma-Aldrich	Cat#A7906
Mouse IL-2	Peprotech	Cat#210–21
Mouse IL-6	Peprotech	Cat#216–16
Mouse IL-10	Peprotech	Cat#210–10
2-mercaptoethanol	Gibco	Cat#31350010
HEPES	Gibco	Cat#15630080
RNasin Plus RNase inhibitor	Promega	Cat#N2111
Luminata HRP substrate	Millipore	Cat#WBLUR0100
Histopaque 1119	Sigma	Cat#11191
ExoSAP-IT	ThermoFisher Scientific	Cat#78201
Paraformaldehyde	Electron Microscopy Sciences	Cat#15714
Protein G IgG Binding Buffer	Thermo Scientific	Cat#21011
Protein G	Cytiva	Cat#17061801
Saponin	Sigma-Aldrich	Cat#84510
Sheep red blood cells	Lampire	Cat#7249008
PVDF	Roche	Cat#3010040001
Carboxymethylcellulose sodium salt	Sigma-Aldrich	Cat#C5013
TrueBlue peroxidase	SeraCare	Cat#5510–0030
Critical Commercial Assays		
Q5 High-Fidelity DNA polymerase	New England Biolabs	Cat#M0491L
Phusion High-Fidelity DNA polymerase	ThermoFisher Scientific	Cat#F549XL
T4 DNA ligase	New England Biolabs	Cat#M0202L
Chromium Single Cell 5’ Library & Gel Bead Kit	10x Genomics	Cat#PN-1000014
Chromium Single Cell V(D)J Enrichment Kit, Mouse B cell	10x Genomics	Cat#PN-1000072
Anti-PE microbeads	Miltenyi Biotec	Cat#130-048-801
NucleoSpin RNA XS isolation kit	Macherey-Nagel	Cat#740990.50
Gel/PCR DNA fragment extraction kit	IBI Scientific	Cat#IB47010
SuperScript III first strand synthesis system	Invitrogen	Cat#18080051
Anti-APC microbeads	Miltenyi Biotec	Cat#130-090-855
Anti-FITC microbeads	Miltenyi Biotec	Cat#130-048-701
LS columns	Miltenyi Biotec	Cat#130-042-401
Deposited Data		
Single cell RNA seq data	This paper	GEO:GSE154102
Experimental Models: Cell Lines		
3T3 mCD40Lhi mBAFF	Purtha et al, 2011	N/A
Lenti-X 293T	Takara	Cat#632180
Vero	ATCC	ATCC CCL-81, RRD: CVCL_0059
Experimental Models: Organisms/Strains		
Mouse: C57BL/6N	Charles River Labs	Strain code 027

Author Manuscript Author Manuscript Author Manuscript Author Manuscript

REAGENT or RESOURCE	SOURCE	IDENTIFIER
Mouse: *Aicda*$^{tm1a(EUCOMM)Hmgu}$	EUCOMM	HEPD0615_4_B08
Mouse: B6(Cg)-Tyrc-2J/J	Jackson Labs	JAX: 000058; RRID:IMSR_JAX:000058
Mouse: 129S4/SvJaeSor-Gt(ROSA)26Sortm1(FLP1)Dym/J	Jackson Labs	JAX: 003946; RRID:IMSR_JAX:003946
Mouse: hCD20-TamCre	Khalil et al., 2012	N/A
Mouse: JchainCreERT2	This paper	N/A
Mouse: B6.Cg-Gt(ROSA)26Sortm14(CAG-tdTomato)Hze/J	Jackson Labs	JAX: 007914; RRID:IMSR_JAX:007914
Oligonucleotides		
Index seq: GATCGGAAGAGCACACGTCTGAACTCCAGTCAC	Sigma	N/A
Primers for genotyping *Aicda*$^{tm1a(EUCOMM)Hmgu}$ mice, see Table S3 (Aicda_237918_F, Aicda_237918_R, CAS_R1_Term)	Genome Research Limited	N/A
Primers for genotyping JchainCreERT2 mice, see Tabls S3 (Jchain WT_F, Jchain Tg_F, Jchain common_R)	This paper	N/A
Murine CpG: TCCATGACGTTCCTGATGCT	Integrated DNA technologies	N/A
msVHEstdseq1: ACACTCTTTCCCTACACGACGCTCTTCCGATCTGGGAATTCG AGGTGCAGCTGCAGGAGTCTGG	This paper	N/A
commonCgstdseq2: GTGACTGGAGTTCAGACGTGTGCTCTTCCGATCTCARKGGAT RRRCHGATGGGG	This paper	N/A
P5 forward Stdseq: AATGATACGGCGACCACCGAGATCTACACTCTTTCCCTACAC GACGC	Lam et al., 2018	N/A
P7 reverse Stdseq index: CGGCATACGAGATNNNNNNNNGTG ACTGGAGTTCAGACGTGTGTG where N represents a unique index for multiplexing.	Lam et al., 2018	N/A
B cell receptor cloning primers	Tiller et al., 2018	Table 2 and Table 3 from Tiller et al., 2018.
Recombinant DNA		
Plasmid: pet21a WNV WT DIII AviTag	This paper, modified from, Oliphant et al., 2007	N/A
Plasmid: pet21a WNV KT DIII AviTag	This paper, modified from, Oliphant et al., 2007	N/A
Plasmid: pet21a JEV WT DIII AviTag	This paper, modified from Fernandez et al., 2018.	N/A
Plasmid: pet21a JEV ESAK DIII AviTag	This paper	N/A
AbVec2.0-IGHGH1	Tiller et al., 2008	Addgene Plasmid#80795
AbVec2.0-IGHGH1-AviTag	This paper, modified from Addgene Plasmid#80795	N/A
AbVec1.1-IGKC	Tiller et al., 2008	Addgene Plasmid#80796
WNV prM-E	Zhang et al., 2016	N/A
Software and Algorithms		
FlowJo v10	BD	https://www.flowjo.com/solutions/flowjo/downloads; RRID:SCR_008520
Prism 8	Graphpad	https://www.graphpad.com/; RRID:SCR_002798

Author Manuscript Author Manuscript Author Manuscript Author Manuscript

REAGENT or RESOURCE	SOURCE	IDENTIFIER
Seurat	Stuart et al., 2019	https://satijalab.org/seurat/install.html; RRID:SCR_007322
BioCircos	Cui et al., 2016	https://cran.r-project.org/web/packages/BioCircos/vignettes/BioCircos.html
IMGT/HighV-Quest	Lefranc et al., 2009	http://www.imgt.org/IMGTindex/IMGTHighV-QUEST.php; RRID:SCR_018196
Cellranger	10x Genomics	https://support.10xgenomics.com/single-cell-gene-expression/software/downloads/latest
The R project for statistical computing	N/A	https://www.r-project.org/
ImmunoSpot S6 Analyzer	Cellular Technology Limited	http://www.immunospot.com/ImmunoSpot-analyzers-software; RRID:SCR_011082
ForteBio DataAnalysis v11.0 software	ForteBio	https://www.fortebio.com/products/octet-systems-software
Migmap	Shugay et al, 2015	https://github.com/mikessh/migmap
Rscrublet	Wolock et al., 2019	https://rdrr.io/github/ChengxiangQiu/rscrublet/
PEAR	Zhang et al., 2014	http://www.exelixis-lab.org/web/software/pear
Other		
Innovator WNV Vaccine	Valley Vet Supply	Cat#39708
Ixiaro JEV vaccine	VaccineShoppe	Cat#42515-002-01
MultiScreen HTS HA Filter Plate	Millipore	MSHAN4510
AddaVax	Invivogen	vac-adx-10
Streptavidin biosensors	ForteBio	Cat#18–5020